

Improving the Sampling Strategy in KernelSHAP

Lars Henry Berge Olsen^{*1} and Martin Jullum²

¹Department of Mathematics, University of Oslo

²Norwegian Computing Center

October 8, 2024

Abstract

Shapley values are a popular model-agnostic explanation framework for explaining predictions made by complex machine learning models. The framework provides feature contribution scores that sum to the predicted response and represent each feature’s importance. The computation of exact Shapley values is computationally expensive due to estimating an exponential amount of non-trivial conditional expectations. The `KernelSHAP` framework enables us to approximate the Shapley values using a sampled subset of weighted conditional expectations. We propose three main novel contributions: a stabilizing technique to reduce the variance of the weights in the current state-of-the-art strategy, a novel weighing scheme that corrects the Shapley kernel weights based on sampled subsets, and a straightforward strategy that includes the important subsets and integrates them with the corrected Shapley kernel weights. We compare these new approximation strategies against existing ones by evaluating their Shapley value accuracy as a function of the number of subsets. The results demonstrate that our sampling strategies significantly enhance the accuracy of the approximated Shapley value explanations, making them more reliable in practical applications. This work provides valuable insights and practical recommendations for researchers and practitioners seeking to implement Shapley value-based explainability of their models.

Keywords: Explainable artificial intelligence, Shapley values, model-agnostic explanation, prediction explanation, feature dependence

1 Introduction

The field of Explainable Artificial Intelligence (XAI) has developed various explanation frameworks to provide insights into the inner workings of complex models and to make their predictions more understandable to humans (Adadi and Berrada 2018; Covert et al. 2021; Molnar 2022). Developing and adopting XAI frameworks is crucial for bridging the gap between model complexity and transparency, trustworthiness, and explainability. When properly used, XAI can foster better decision-making, ensure compliance with regulatory standards, and facilitate model debugging by enabling practitioners/stakeholders to comprehend their model’s decision-making process (Ebers 2020; Schwalbe and Finzel 2023). As machine learning continues to evolve, the role of XAI will become increasingly important in ensuring that the benefits of advanced models are harnessed responsibly and effectively. One of the most used explanation frameworks is *Shapley values* (Shapley 1953; Molnar 2023).

^{*}E-mail address to corresponding author: lholsen@math.uio.no.

Shapley values stem from cooperative game theory but are in the context of XAI, often used as a *post-hoc model-agnostic local* explanation framework that explains the prediction $f(\mathbf{x})$ made by a complex model f . Post-hoc means that the explanations are made after the model has been trained and its predictions made. That is, the explanations are not inherently built into the model but are derived from its behavior. Model-agnostic means that we can explain any model f , and local means that we explain the prediction of a single observation \mathbf{x} called the *explicand*. The explanation is a vector of feature contributions ϕ that sums to the predicted response.

In this paper, we consider the setting of supervised learning and provide Shapley values to explain a predictive model $f(\mathbf{x})$ trained on $\mathcal{X} = \{\mathbf{x}^{[i]}, y^{[i]}\}_{i=1}^{N_{\text{train}}}$. Here $\mathbf{x}^{[i]}$ is an M -dimensional feature vector, $y^{[i]}$ is a univariate response, and N_{train} is the number of training observations. However, Shapley values can be extended to provide *global explanations*, i.e., explaining global model effects across all observations (Owen 2014; Covert et al. 2020; Frye et al. 2021), and to other domains: images (Jethani et al. 2021), text (Chen et al. 2018), graphs (Wang et al. 2021; Duval and Malliaros 2021), and series of models (Chen et al. 2022b). Molnar (2022) provides a detailed overview and introduction to other explanation frameworks such as *accumulated local effects*, *local interpretable model-agnostic explanations*, and *counterfactual explanations*.

We focus on *conditional Shapley values*, which incorporates feature dependencies into the explanations (Aas et al. 2021a). This is in contrast to *marginal Shapley values* where one omits the dependencies. The two versions coincide when there are no dependencies between features, and the methods proposed in this paper also apply to marginal Shapley values. The conditional Shapley values are consistent with standard probability axioms (Covert et al. 2021, Proposition 7), but this consistency comes at the cost of increased computational complexity due to the necessity of modeling dependencies between arbitrary feature combinations. Throughout this article, we refer to conditional Shapley values when discussing Shapley values unless otherwise specified.

In general, computing Shapley values is an NP-hard problem (Deng and Papadimitriou 1994; Faigl and Kern 1992), and the direct computations are exponential in the number of features M . A wide range of approximation strategies have been proposed, which are either based on model assumptions (making the explanations *model-specific*) or model-agnostic methods that use stochastic, sampling-based estimators that are correct in expectation. The model-agnostic methods are connected to different but equivalent formulations of Shapley values. Shapley values can be viewed as a *semivalue* (Castro et al. 2009), *least squares value* (Charnes et al. 1988), *random order value* (Monderer and Samet 2002), or a *multilinear extension* (Owen 1972). See Chen et al. (2023) for a more in-depth introduction to these Shapley value formulations.

We compute Shapley values by solving a weighted least squares problem, thus focusing on approximation strategies tied to the least squares value formulation. More specifically, we propose enhancements to the `KernelSHAP` approximation framework (Lundberg and Lee 2017) and the current state-of-the-art strategy (Covert et al. 2021) to lower the computational complexity and improve the tractability. `KernelSHAP` approximates Shapley values using a (weighted) subset of the exponential number of feature combinations. We introduce novel strategies to select and weigh the elements of this subset using stabilizing techniques and corrected Shapley kernel values based on the sampled subset.

Section 2 introduces the Shapley value explanation framework and how to compute them exactly and approximate them using the `KernelSHAP` framework. Section 3 discusses the current state-of-the-art approximation strategies and our novel extensions and strategies. Section 4 presents numerical simulation studies comparing the accuracy of the different approximation strategies, while Section 5 conducts experiments on real-world data. Finally, Section 6 provides conclusions and outlines further work. The Appendix includes implementation details, other strategies, and additional information.

2 Shapley Values

Shapley values are a solution concept of how to divide the payout of a cooperative game $v : \mathcal{P}(\mathcal{M}) \mapsto \mathbb{R}$ onto the players based on four axioms (Shapley 1953). The game is played by M players where $\mathcal{M} = \{1, 2, \dots, M\}$ denotes the set of all players and $\mathcal{P}(\mathcal{M})$ is the power set, that is, the set of all

subsets of \mathcal{M} . We call $v(\mathcal{S})$ the *contribution function*¹ and it maps a subset of players $\mathcal{S} \in \mathcal{P}(\mathcal{M})$, also called a *coalition*, to a real number representing their contribution in the game v . In model explanation, the predictive model f (indirectly) replaces the cooperative game, the j th feature x_j represents the j th player, and the payout is the predicted response $f(\mathbf{x})$. This is done for a specific explicand $\mathbf{x} = \mathbf{x}^*$.

The Shapley values $\phi_j = \phi_j(v)$ assigned to each feature j , for $j = 1, \dots, M$, uniquely satisfy the following properties:

Efficiency: They sum to the value of the grand coalition \mathcal{M} minus the empty set \emptyset , that is, $\sum_{j=1}^M \phi_j = v(\mathcal{M}) - v(\emptyset) = f(\mathbf{x}) - \mathbb{E}[f(\mathbf{x})]$.

Symmetry: Two equally contributing features j and k , that is, $v(\mathcal{S} \cup \{j\}) = v(\mathcal{S} \cup \{k\})$ for all \mathcal{S} , receive equal payouts $\phi_j = \phi_k$.

Dummy: A non-contributing feature j , that is, $v(\mathcal{S}) = v(\mathcal{S} \cup \{j\})$ for all \mathcal{S} , receives $\phi_j = 0$.

Linearity: A linear combination of n games $\{v_1, \dots, v_n\}$, that is, $v(\mathcal{S}) = \sum_{k=1}^n c_k v_k(\mathcal{S})$, has Shapley values given by $\phi_j(v) = \sum_{k=1}^n c_k \phi_j(v_k)$.

Shapley (1953) showed that the values ϕ_j which uniquely satisfy these axioms are given by

$$\phi_j = \sum_{\mathcal{S} \in \mathcal{P}(\mathcal{M} \setminus \{j\})} \frac{|\mathcal{S}|!(M - |\mathcal{S}| - 1)!}{M!} (v(\mathcal{S} \cup \{j\}) - v(\mathcal{S})), \quad (1)$$

where $|\mathcal{S}|$ is the number of features in coalition \mathcal{S} . The number of terms in (1) is 2^M , hence, the complexity grows exponentially with the number of features M . The Shapley value ϕ_j is a weighted average of the j th feature's marginal contribution to each coalition \mathcal{S} and describes the importance of the j th feature in the prediction $f(\mathbf{x}^*) = \phi_0 + \sum_{j=1}^M \phi_j^*$, where $\phi_0 = \mathbb{E}[f(\mathbf{x})]$. That is, the sum of the Shapley values explains the difference between the prediction $f(\mathbf{x}^*)$ and the global average prediction.

To compute (1), we need to define an appropriate contribution function $v(\mathcal{S}) = v(\mathcal{S}, \mathbf{x}^*)$ that should resemble the value of $f(\mathbf{x}^*)$ when only the features in coalition \mathcal{S} are known. In the conditional Shapley value explanation framework, the contribution function $v(\mathcal{S})$ is the expected response of $f(\mathbf{x})$ conditioned on the features in \mathcal{S} taking on the values $\mathbf{x}_{\mathcal{S}}^*$ (Lundberg and Lee 2017). That is,

$$v(\mathcal{S}) = \mathbb{E}[f(\mathbf{x}) | \mathbf{x}_{\mathcal{S}} = \mathbf{x}_{\mathcal{S}}^*] = \mathbb{E}[f(\mathbf{x}_{\bar{\mathcal{S}}}, \mathbf{x}_{\mathcal{S}}) | \mathbf{x}_{\mathcal{S}} = \mathbf{x}_{\mathcal{S}}^*] = \int f(\mathbf{x}_{\bar{\mathcal{S}}}, \mathbf{x}_{\mathcal{S}}^*) p(\mathbf{x}_{\bar{\mathcal{S}}} | \mathbf{x}_{\mathcal{S}} = \mathbf{x}_{\mathcal{S}}^*) d\mathbf{x}_{\bar{\mathcal{S}}}, \quad (2)$$

where $\mathbf{x}_{\mathcal{S}} = \{x_j : j \in \mathcal{S}\}$ denotes the features in subset \mathcal{S} , $\mathbf{x}_{\bar{\mathcal{S}}} = \{x_j : j \in \bar{\mathcal{S}}\}$ denotes the features outside \mathcal{S} , that is, $\bar{\mathcal{S}} = \mathcal{M} \setminus \mathcal{S}$, and $p(\mathbf{x}_{\bar{\mathcal{S}}} | \mathbf{x}_{\mathcal{S}} = \mathbf{x}_{\mathcal{S}}^*)$ is the conditional density of $\mathbf{x}_{\bar{\mathcal{S}}}$ given $\mathbf{x}_{\mathcal{S}} = \mathbf{x}_{\mathcal{S}}^*$. The conditional expectation summarizes the whole probability distribution, it is the most common estimator in prediction applications, and it is also the minimizer of the commonly used squared error loss function (Aas et al. 2021a). Note that the last equality of (2) only holds for continuous features. If there are any discrete or categorical features, the integral should be replaced by sums for these features. Hence, $p(\mathbf{x}_{\bar{\mathcal{S}}} | \mathbf{x}_{\mathcal{S}} = \mathbf{x}_{\mathcal{S}}^*)$ is then no longer continuous.

To compute the Shapley values in (1), we need to compute (2) for all $\mathcal{S} \in \mathcal{P}(\mathcal{M})$, except for the edge cases $\mathcal{S} \in \{\emptyset, \mathcal{M}\}$. For $\mathcal{S} = \emptyset$, we have by definition that $\phi_0 = v(\emptyset) = \mathbb{E}[f(\mathbf{x})]$, where the average training response \bar{y}_{train} is a commonly used estimate (Aas et al. 2021a). While for $\mathcal{S} = \mathcal{M}$, $\mathbf{x}_{\mathcal{S}} = \mathbf{x}^*$ and $v(\mathcal{M}) = f(\mathbf{x}^*)$ by definition. We denote the non-trivial coalitions by $\mathcal{P}^*(\mathcal{M}) = \mathcal{P}(\mathcal{M}) \setminus \{\emptyset, \mathcal{M}\}$.

Computing (2) is not straightforward for a general data distribution and model. Assuming independent features, or having f be linear, simplifies the computations (Lundberg and Lee 2017; Aas et al. 2021a), but these assumptions do not generally hold. There is a wide range of methods used to estimate $v(\mathcal{S})$, using, e.g., Gaussian assumptions (Chen et al. 2020; Aas et al. 2021a), conditional inference trees (Redelmeier et al. 2020), or variational auto-encoders (Olsen et al. 2022). Olsen et al. (2024) provides an extensive overview of the methods and categorizes them according to whether they use Monte Carlo integration or regression to estimate the contribution function.

¹It is also called the *value*, *reward*, *lift*, and *characteristic* function in the literature.

In the simulation studies in Section 4, we generate data from the multivariate Gaussian distribution. Thus, we can compute $p(\mathbf{x}_{\bar{S}}|\mathbf{x}_S = \mathbf{x}_S^*)$ and estimate (2) by Monte Carlo integration:

$$v(\mathcal{S}) = v(\mathcal{S}, \mathbf{x}^*) = \mathbb{E}[f(\mathbf{x}_{\bar{S}}, \mathbf{x}_S)|\mathbf{x}_S = \mathbf{x}_S^*] \approx \frac{1}{K} \sum_{k=1}^K f(\mathbf{x}_{\bar{S}}^{(k)}, \mathbf{x}_S^*) = \hat{v}(\mathcal{S}), \quad (3)$$

where f is the predictive model, $\mathbf{x}_{\bar{S}}^{(k)} \sim p(\mathbf{x}_{\bar{S}}|\mathbf{x}_S = \mathbf{x}_S^*)$, for $k = 1, 2, \dots, K$, and $K = 5000$ is the number of Monte Carlo samples. To obtain accurate conditional Shapley values, we need to generate Monte Carlo samples that follow the true conditional distribution of the data.

2.1 Approximation Strategies

In this section, we highlight procedures that use approximations or model assumptions to reduce the computational complexity of the Shapley value explanation framework and make the computations tractable in higher dimensions. The approximative speed-up strategies can be divided into model-specific and model-agnostic strategies (Chen et al. 2023).

The model-specific strategies put assumptions on the predictive model f to improve the computational cost, but some of the strategies are restricted to marginal Shapley values. For conditional Shapley values, Aas et al. (2021a) and Chen et al. (2020) derive explicit expressions for linear models to speed up the computations, and Lundberg et al. (2020) proposes the path-dependent **TreeSHAP** algorithm for tree-based models. Yang (2021) improves the speed of the **TreeSHAP** algorithm by pre-computing expensive steps at the cost of a slightly higher memory consumption. While Bifet et al. (2022) reduce the time complexity from polynomial to linear time with their **Linear TreeSHAP** algorithm and Muschalik et al. (2024) extend it to any-order Shapley interaction index scores (Grabisch and Roubens 1999). There are also speed-up strategies for deep neural network models, but they are limited to marginal Shapley values (Ancona et al. 2019; Wang et al. 2020).

The model-agnostic strategies put no assumptions on the predictive model f and often use stochastic sampling-based estimators (Aas et al. 2021a; Lundberg and Lee 2017; Okhrati and Lipani 2021; Mitchell et al. 2022). That is, to speed up the computations, they approximate the Shapley value explanations by a sampled subset of the coalitions instead of considering the exponential amount of them. Thus, the strategies are stochastic; however, their expectations are unbiased. One of the most common model-agnostic strategies is the **KernelSHAP** strategy introduced in Lundberg and Lee (2017) and improved by Covert and Lee (2021). In the **KernelSHAP** strategy, we sample, e.g., $N_S < 2^M$ coalitions and use only these coalitions to approximate the Shapley value explanations using the least squares value formulation. This strategy enables us to approximate the explanations in tractable time even for large values of M ; however, an $N_S \ll 2^M$ will (likely) produce poor approximations.

There exist other approximation strategies linked to alternative Shapley formulations, such as the permutation sampling-based frameworks based on the random order value formulation (Strumbelj and Kononenko 2010, 2014; Chen et al. 2022a). We prefer the **KernelSHAP** framework over permutation sampling-based frameworks due to its superior efficiency. In the context of conditional Shapley values, the primary computational burden is related to the number of $v(\mathcal{S})$ values that need to be calculated. **KernelSHAP** leverages *all* computed $v(\mathcal{S})$ values to determine the Shapley values for *all* features. In contrast, permutation sampling only uses a portion of the evaluated $v(\mathcal{S})$ values to estimate each feature’s Shapley value, resulting in less efficient utilization of these values. Examples of approximation strategies for the permutation sampling-based framework include orthogonal spherical codes (Mitchell et al. 2022), stratified sampling (Castro et al. 2017; Maleki 2015), paired sampling (Covert and Lee 2021; Mitchell et al. 2022), and many others (Mitchell et al. 2022; Campen et al. 2018; Illés and Kerényi 2019). However, these strategies typically cannot be directly integrated into the **KernelSHAP** approximation framework and are thus considered outside the scope of this article.

We refer to Chen et al. (2023) for more details about the model-agnostic and model-specific strategies. Jethani et al. (2021) propose to sidestep the Shapley value formula by training a black-box neural network to directly output the Shapley value explanations, while Jullum et al. (2021) explain groups of similar/correlated features instead of individual features to reduce the computations.

2.2 The KernelSHAP Framework

Lundberg and Lee (2017) show that the Shapley value formula in (1) may also be conveniently expressed as the solution of the following weighted least squares problem

$$\arg \min_{\phi \in \mathbb{R}^{M+1}} \sum_{\mathcal{S} \in \mathcal{P}(\mathcal{M})} k(M, \mathcal{S}) \left(\phi_0 + \sum_{j \in \mathcal{S}} \phi_j - v(\mathcal{S}) \right)^2, \quad (4)$$

where

$$k(M, |\mathcal{S}|) = \frac{M-1}{\binom{M}{|\mathcal{S}|} |\mathcal{S}| (M-|\mathcal{S}|)}, \quad (5)$$

for $|\mathcal{S}| = 0, 1, 2, \dots, M$, are the *Shapley kernel weights* (Charnes et al. 1988; Lundberg and Lee 2017). In practice, the infinite Shapley kernel weights $k(M, 0) = k(M, M) = \infty$ can be set to a large constant $C = 10^6$ (Aas et al. 2021a). The matrix solution of (4) is

$$\phi = (\mathbf{Z}^T \mathbf{W} \mathbf{Z})^{-1} \mathbf{Z}^T \mathbf{W} \mathbf{v} = \mathbf{R} \mathbf{v}. \quad (6)$$

Here \mathbf{Z} is a $2^M \times (M+1)$ matrix with 1s in the first column (to obtain ϕ_0) and the binary representations² of the coalitions $\mathcal{S} \subseteq \mathcal{M}$ in the remaining columns. While $\mathbf{W} = \text{diag}(C, \mathbf{w}, C)$ is a $2^M \times 2^M$ diagonal matrix containing the Shapley kernel weights $k(M, |\mathcal{S}|)$. The \mathbf{w} vector contains the $2^M - 2$ finite Shapley kernel weights, which we normalize to sum to one for numerical stability. Finally, \mathbf{v} is a column vector of height 2^M containing the contribution function values $v(\mathcal{S})$. The \mathcal{S} in \mathbf{W} and \mathbf{v} corresponds to the coalition of the corresponding row in \mathbf{Z} . The \mathbf{R} matrix is independent of the explicands. When explaining N_{explain} predictions, we can replace \mathbf{v} with a $2^M \times N_{\text{explain}}$ matrix \mathbf{V} , where column i contains the contribution functions for the i th explicand.

Exact computations are infeasible in higher dimensions as the number of coalitions 2^M grows exponentially with the number of features M . A common solution is to approximate the Shapley values by solving (4) using a sampled subset of coalitions $\mathcal{D} \subseteq \mathcal{P}(\mathcal{M})$ (with replacement) instead of all coalitions $\mathcal{S} \in \mathcal{P}(\mathcal{M})$. This framework is called **KernelSHAP** (Lundberg and Lee 2017), and the coalitions are sampled from a distribution following the Shapley kernel weights in (6). Thus, the sampled subsets are weighted equally in the new weighted least squares problem, while the empty and grand coalitions are always included and exempt from the sampling. The corresponding Shapley value approximation is

$$\phi_{\mathcal{D}} = (\mathbf{Z}_{\mathcal{D}}^T \mathbf{W}_{\mathcal{D}} \mathbf{Z}_{\mathcal{D}})^{-1} \mathbf{Z}_{\mathcal{D}}^T \mathbf{W}_{\mathcal{D}} \mathbf{v}_{\mathcal{D}}, \quad (7)$$

where only the $N_{\mathcal{S}} = |\mathcal{D}|$ unique coalitions in \mathcal{D} are used. If a coalition \mathcal{S} is sampled K times, then the corresponding weight in $\mathbf{W}_{\mathcal{D}} = \text{diag}(C, \mathbf{w}_{\mathcal{D}}, C)$, denoted by $w_{\mathcal{S}}$, is proportional to K , as we normalize the weights for numerical stability. The **KernelSHAP** framework is also useful in lower dimensions if $v(\mathcal{S})$ is expensive to compute. Williamson and Feng (2020) shows that the **KernelSHAP** approximation framework is consistent and asymptotically unbiased, while Covert and Lee (2021) shows that it is empirically unbiased for even a modest number of coalitions.

3 Sampling Strategies

In this section, we describe established and novel strategies for selecting the $N_{\mathcal{S}}$ unique coalitions in \mathcal{D} and how to weigh them in (7) when approximating Shapley value explanations. We provide an overview of the strategies and their characteristic properties in Table 1. The empty and grand coalitions are always included in the approximations; thus, they are excluded from the sampling procedure. Consequently, $N_{\mathcal{S}}$ is an integer between (exclusive) 2 and 2^M , as the full set of coalitions yields exact Shapley values. In Appendix E, we discuss alternative strategies that were investigated but performed worse. In Appendix G, we demonstrate that our novel techniques can significantly enhance the strategy used in the **SHAP** Python library (Lundberg and Lee 2024).

²For example, the binary representation of $\mathcal{S} = \{1, 3\}$ in an $M = 4$ -dimensional setting is $[1, 0, 1, 0]$.

Strategy	Stochastic sampling	Paired sampling	Equal weights within each coalition size	Deterministic weights	Weight w_S converges to p_S	Weight w_S is proportional to
Unique	✓	✗	✗	✗	~	$\#(\mathcal{S})$
Paired	✓	✓	✗	✗	~	$\#(\mathcal{S} \text{ or } \bar{\mathcal{S}})$
Paired average	✓	✓	✓	✗	✓	$\sum_{\mathcal{T} \in \mathcal{P}(\mathcal{M})_{ \mathcal{S} }} \#(\mathcal{T}) / N_{\mathcal{D}, \mathcal{S} }$
Paired kernel	✓	✓	✓	✓	✓	p_S
Paired c-kernel	✓	✓	✓	✗	✓	$2p_S / (1 - (1 - 2p_S)^{L/2})$
Paired cel-kernel	✓	✓	✓	✓	✓	$2p_S / (1 - (1 - 2p_S)^{\mathbb{E}[L]/2})$
Paired imp c-kernel	~	✓	✓	✗	✗	$2p_S / (1 - (1 - 2p_S)^{N_S/2})$
Paired imp cel-kernel	~	✓	✓	✓	✓	$2p_S / (1 - (1 - 2p_S)^{\mathbb{E}[L]/2})$

Table 1: Overview of the strategies introduced in Section 3 together with the weight w_S they give to coalition \mathcal{S} in (7). **Stochastic sampling**: all strategies stochastically sample (with replacement) the coalition set \mathcal{D} , except the **paired imp** strategies, which includes the most important coalitions first and only sample (without replacement) within the coalition size where not all coalitions are included. **Paired sampling**: whether the strategy samples the paired coalitions \mathcal{S} and $\bar{\mathcal{S}}$ together. **Equal weights within each coalition size**: whether coalitions of the same size have the same weight. **Deterministic weights**: whether the weights are deterministically determined by the number of features M or if they depend on the sampled coalitions. **Weight w_S converges to p_S** : whether the weight w_S converges to p_S in (8) when $N_S \rightarrow 2^M$. The **unique** and **paired** strategies converge in theory, but the convergence is slow in practice due to large weight variability; see Figure 1. **Weight w_S is proportional to**: specifies the proportional weight w_S given to coalition \mathcal{S} in (7). The $\#(\mathcal{S})$ notation should be read as “the number of times \mathcal{S} is sampled”, $\mathcal{P}(\mathcal{M})_{|\mathcal{S}|} = \{\mathcal{R} \in \mathcal{P}(\mathcal{M}) \mid |\mathcal{R}| = |\mathcal{S}|\}$, and $N_{\mathcal{D}, |\mathcal{S}|}$ is the number of unique coalitions in \mathcal{D} with size $|\mathcal{S}|$. While L is the total number of coalitions sampled such that \mathcal{D} contains N_S unique coalitions, $\mathbb{E}[L]$ is the expected value of L , and $p_S \propto k(M, |\mathcal{S}|)$ as defined in (8).

In Figures 1 and 2, we illustrate the weights used in (7) by the strategies introduced below when normalized over the N_S unique coalitions in \mathcal{D} . Figure 1 focuses on an $M = 10$ -dimensional setting with $N_S \in \{100, 250, 750, 1000\}$. We index the coalitions by first ordering them based on coalition size, i.e., $\{1\}$ precedes $\{1, 2\}$, and then by their elements for equal-sized coalitions, i.e., $\{1, 2\}$ precedes $\{1, 3\}$. This indexing ensures that coalitions with indices i and $2^M + 1 - i$ are complementary, for $i = 1, 2, \dots, 2^M$, as seen by the **paired** strategy’s weights being symmetric around the dashed vertical lines in Figure 1. The weights of the empty ($i = 1$) and grand ($i = 2^M = 1024$) coalitions are omitted as they are strategy-independent and infinite.

3.1 Unique

To obtain N_S unique coalitions, the **unique** strategy samples a sequence of $L \geq N_S$ coalitions with replacements from the Shapley kernel weight distribution

$$p_S = p(\mathcal{S}) = \frac{k(M, |\mathcal{S}|)}{\sum_{\mathcal{S} \in \mathcal{P}^*(\mathcal{M})} k(M, |\mathcal{S}|)} = \frac{k(M, |\mathcal{S}|)}{\sum_{q=1}^{M-1} k(M, q) \binom{M}{q}}, \quad (8)$$

where $k(M, |\mathcal{S}|)$ is the Shapley kernel weight given in (5). We determine the coalitions using a two-step procedure to avoid listing all $|\mathcal{P}^*(\mathcal{M})| = 2^M - 2$ coalitions. First, we sample the coalition sizes $|\mathcal{S}| \in \{1, \dots, M - 1\}$ using weighted sampling with replacement, where the weights are $k(M, |\mathcal{S}|) \binom{M}{|\mathcal{S}|}$. Second, we uniformly sample $|\mathcal{S}|$ of the M features without replacement. We repeat this procedure L times until we have N_S unique coalitions, which will constitute \mathcal{D} . We use the sampling frequencies as the weights w_S in (7) as some coalitions might have been sampled multiple times. That is,

$$w_S \propto \#(\mathcal{S}), \quad (9)$$

where the $\#(\mathcal{S})$ notation should be read as “the number of times coalition \mathcal{S} is sampled”. This strategy was outlined by Lundberg and Lee (2017) and Aas et al. (2021a).

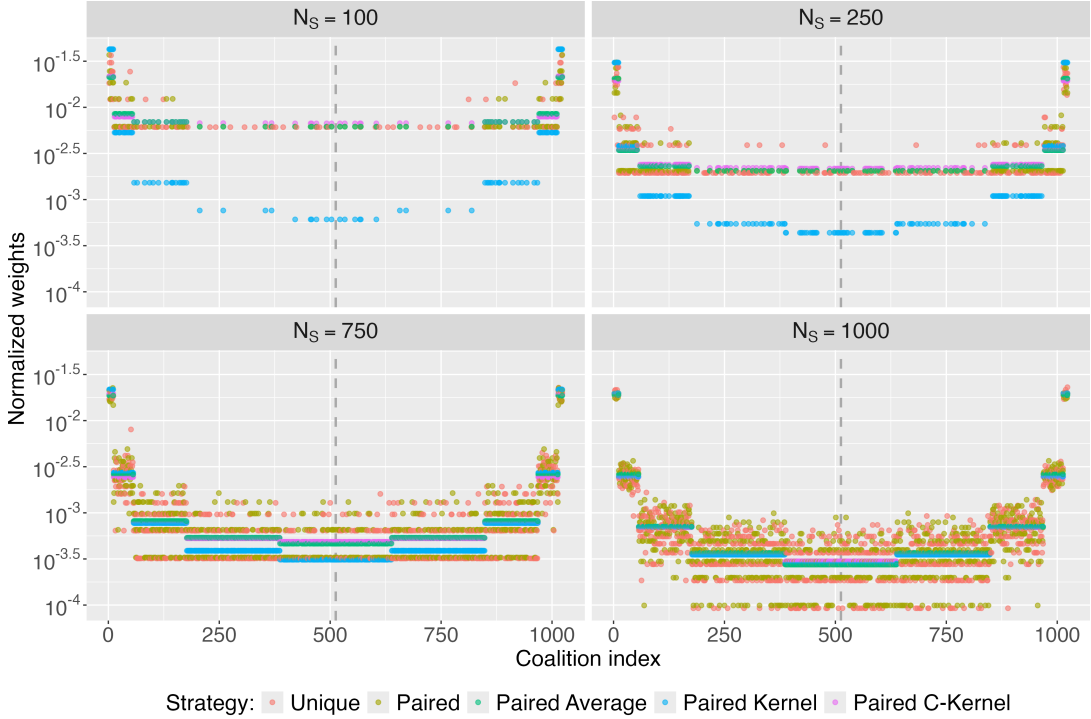


Figure 1: The normalized weights w_S used in (7) by the first five strategies in Section 3 for different number of unique coalitions N_S in an $M = 10$ -dimensional setting. The **paired** and **paired average** strategies are overlapping for $|\mathcal{S}| \in \{4, 5, 6\}$ when $N_S \in \{100, 250\}$. The **paired**-based strategies are symmetric around the vertical line. The **paired average** strategy has identical weights within each coalition size, and they are slightly different from the weights in the **paired c-kernel** strategy.

3.2 Paired

The **paired** strategy improves the **unique** strategy by using a variance reduction technique for Monte Carlo methods called *paired sampling*³ (Kroese et al. 2013, Ch. 9). Covert and Lee (2021) demonstrates that paired sampling reduces the variance of the Shapley values approximations compared to the **unique** strategy. The **paired** sampling strategy pairs each sampled coalition \mathcal{S} , determined by the **unique** strategy, with its complement/inverse $\bar{\mathcal{S}} = \mathcal{M} \setminus \mathcal{S}$. Without loss of generality, let \mathcal{S} be the smaller set of \mathcal{S} and $\bar{\mathcal{S}}$, and $\bar{\mathcal{S}}$ the larger. This will be useful in the remainder of the paper when we talk about coalition size as then $|\mathcal{S}| \leq \lfloor M/2 \rfloor$, where $\lfloor \cdot \rfloor$ denotes the floor function. Conceptually, we only sample coalitions \mathcal{S} with coalition indices less than or equal to 2^{M-1} and then add their paired counterparts $\bar{\mathcal{S}}$ with coalition indices larger than 2^{M-1} . The probability of sampling \mathcal{S} is then $p_S + p_{\bar{\mathcal{S}}} = 2p_S$, where p_S is given in (8). However, the doubling is redundant when normalizing the probabilities, as all coalitions have doubled their probability. Note that N_S will always be an even number for the **paired** strategy. The **paired** strategy also stabilizes the sampling frequencies by ensuring that \mathcal{S} and $\bar{\mathcal{S}}$ always obtain the same weights, as seen in Figure 1. The weights are given by

$$w_S \propto \#(\mathcal{S} \text{ or } \bar{\mathcal{S}}), \quad (10)$$

where $\#(\mathcal{S} \text{ or } \bar{\mathcal{S}})$ should be read as “the number of times \mathcal{S} or $\bar{\mathcal{S}}$ has been sampled”.

³Also called *antithetic* and *halved* sampling in the literature (Chen et al. 2023).

3.3 Paired Average

We propose to further decrease the variance of the weights w_S by stabilizing the sampling frequencies not only between paired coalitions but also within each coalition size. We name the strategy for **paired average** as we achieve this by averaging the sampling frequencies of the sampled coalitions within each coalition size. This means that the stabilized weights w_S are given by

$$w_S \propto \frac{\sum_{\mathcal{T} \in \{\mathcal{R} \in \mathcal{P}(\mathcal{M}) \mid |\mathcal{R}| = |\mathcal{S}|\}} \#(\mathcal{T})}{\sum_{\mathcal{T} \in \mathcal{D}} \mathbb{1}(|\mathcal{T}| = |\mathcal{S}|)} = \frac{\sum_{\mathcal{T} \in \mathcal{P}(\mathcal{M})_{|\mathcal{S}|}} \#(\mathcal{T})}{N_{\mathcal{D}, |\mathcal{S}|}}, \quad (11)$$

where $\mathcal{P}(\mathcal{M})_{|\mathcal{S}|} = \{\mathcal{R} \in \mathcal{P}(\mathcal{M}) \mid |\mathcal{R}| = |\mathcal{S}|\}$, $\mathbb{1}$ is the indicator function, and $N_{\mathcal{D}, |\mathcal{S}|} = \sum_{\mathcal{T} \in \mathcal{D}} \mathbb{1}(|\mathcal{T}| = |\mathcal{S}|)$ is the number of unique coalitions in the sampled subset $\mathcal{D} \subset \mathcal{P}(\mathcal{M})$ with size $|\mathcal{S}|$. Note that the coalition sizes $|\mathcal{S}|$ and $|\bar{\mathcal{S}}| = M - |\mathcal{S}|$ will have identical weights as we apply **paired** sampling. The **paired** and **paired average** strategies are identical for coalition sizes where no coalition has been sampled more than once. The **paired average** sampling strategy is more stable and its weights tend faster to p_S in (8) when $N_S \rightarrow 2^M$ than the **unique** and **paired** strategies; see Figure 1. To the best of our knowledge, the **paired average** strategy is a novel extension to the **paired** strategy.

A natural extension to reduce the variance of the weights w_S further is to repeat the sampling step B times and use the empirical means of (11) as the new and more stable weights. We include this strategy in Appendix E and call it **paired empirical**. However, the performance is more or less identical to the **paired c-kernel** strategy, which we introduce below in Section 3.5.

3.4 Paired Kernel

As the weights of the **paired average** strategy tend to the normalized Shapley kernel weights p_S given in (8) and the exact Shapley value computations use these weights, a natural consideration is to also use these directly as weights when we approximate the Shapley values. In the **paired kernel** strategy, we sample the coalitions as in the **paired** strategy, but we let the weights be

$$w_S \propto p_S. \quad (12)$$

See Table 2 for the values of p_S for some dimensionalities. Coalitions of equal size have the same weight in the **paired kernel** strategy. In Appendix B, we demonstrate and explore the relation between the **paired average** and **paired kernel** strategies.

3.5 Paired C-Kernel

The **paired c-kernel** strategy corrects the weights in the **paired kernel** strategy by conditioning on the coalitions being sampled at least once. For ease of understanding, we first explain the correction technique for the **unique** setting before we extend it to the **paired** setting, which is the one we use.

The **unique** strategy samples a sequence of $L \geq N_S$ coalitions with replacements until N_S unique coalitions are obtained. The probability of sampling a coalition \mathcal{S} with size $|\mathcal{S}|$ is p_S given by (8). In the **paired kernel** strategy, we directly use the p_S quantities as weights, but we do not condition on \mathcal{S} being among the N_S uniquely sampled coalitions, which is additional information that naturally should be reflected in the weights. When we consider this, we get the corrected Shapley kernel weights

$$\tilde{p}_S = \frac{p_S}{\Pr(\mathcal{S} \text{ sampled at least once})} = \frac{p_S}{1 - \Pr(\mathcal{S} \text{ not sampled})} = \frac{p_S}{1 - (1 - p_S)^L}, \quad (13)$$

which we normalize to sum to one over the non-trivial coalitions.

In Section 3.2, we discussed that **paired** sampling conceptually only samples coalitions \mathcal{S} with coalition indices less than or equal to 2^{M-1} and then add the paired $\bar{\mathcal{S}}$. Thus, the number of sampling steps L is halved while the corresponding probabilities become $2p_S$. The **paired** equivalent of (13) is

$$\tilde{p}_S = \frac{2p_S}{\Pr(\mathcal{S} \text{ and } \bar{\mathcal{S}} \text{ sampled at least once})} = \frac{2p_S}{1 - (1 - 2p_S)^{L/2}}, \quad (14)$$

which means that the weight w_S given by the **paired c-kernel** strategy to coalition S in (7) is

$$w_S \propto \frac{2p_S}{1 - (1 - 2p_S)^{L/2}}. \quad (15)$$

Note that the normalization means that the two in the numerator in (14) and (15) is redundant.

The **paired c-kernel** strategy assigns equal weight to coalitions within the same coalition size and between paired coalition sizes $|\mathcal{S}|$ and $|\bar{\mathcal{S}}| = M - |\mathcal{S}|$, as illustrated in Figure 1. Note that (15) is not a fully analytical expression, as we need to sample a sequence of coalitions to obtain L . However, there is no additional computational cost since sampling a subset of coalitions is already required when approximating Shapley values. Nevertheless, different L values are obtained each time due to the stochastic nature of the sampling process, which results in slightly different \tilde{p}_S values, as represented by the confidence bands in Figure 2.

3.6 Paired CEL-Kernel

The **paired cel-kernel** strategy extends the **paired c-kernel** strategy by replacing L in (14) with the expected value $\mathbb{E}[L] = \mathbb{E}[L \mid N_S \text{ unique coalitions}]$. This removes the variability in the **paired c-kernel** strategy caused by the stochastic L . We use results related to the *coupon collector's problem* (Ferrante and Saltalamacchia 2014) from combinatorial probability theory to obtain the theoretically expected number of samples L needed to obtain N_S unique coalitions.

For ease of understanding, we first introduce the results for the **unique** setting before we extend it to the **paired** setting. In the **unique** setting, we consider the coalitions to be coupons with non-uniform probabilities of being collected, and we want to collect a subset of the $2^M - 2$ coupons / non-trivial coalitions. This is a generalization of the classical coupon collector's problem, which focuses on the expected number of draws it takes to collect all coupons when they have an equal probability of being collected. For our general setting, Flajolet et al. (1992, Corollary 4.2) proves that

$$\mathbb{E}[L] = \mathbb{E}[L \mid N_S \text{ unique coalitions}] = \sum_{q=0}^{N_S-1} (-1)^{N_S-1-q} \binom{2^M - 2 - q - 1}{2^M - 2 - N_S} \sum_{|\mathcal{T}|=q} \frac{1}{1 - P_{\mathcal{T}}}, \quad (16)$$

where $\sum_{|\mathcal{T}|=q}$ is the sum over all sets of coalitions that contain q unique coalitions and $P_{\mathcal{T}} = \sum_{S \in \mathcal{T}} p_S$. The p_S quantity represents the probability of sampling coalition S and is given in (8).

In the **paired** setting, we sample $\tilde{N}_S = N_S/2$ paired coalitions to obtain N_S total coalitions, where N_S is even. The probability of sampling the paired coalitions S and \bar{S} is $2p_S$ while the total number of non-trivial paired coalitions is $2^{M-1} - 1$. The **paired** equivalent to (16) is therefore given by

$$\mathbb{E}[L] = 2 \sum_{q=0}^{\tilde{N}_S-1} (-1)^{\tilde{N}_S-1-q} \binom{2^{M-1} - 1 - q - 1}{2^{M-1} - 1 - \tilde{N}_S} \sum_{|\mathcal{T}|=q} \frac{1}{1 - P_{\mathcal{T}}}, \quad (17)$$

where $\sum_{|\mathcal{T}|=q}$ represents the sum over all sets of paired coalitions that contain q unique paired coalitions and $P_{\mathcal{T}} = \sum_{S \in \mathcal{T}} 2p_S$. Furthermore, we multiply by two at the beginning of (17) because each paired coalition contains two individual coalitions. Computing (17) is not computationally trivial, as the right-most sum in (17) contains $\binom{2^{M-1}-1}{q}$ terms representing the subsets containing q unique paired coalitions. The binomial coefficient is bounded by $\mathcal{O}(2^{2^M}/\sqrt{2^M})$ when 2^M tends to infinity.

We propose a reformulation of (17) which drastically reduces the number of terms by grouping coalitions with equal probability together. This idea exploits that $P_{\mathcal{T}}$ only depends on the number of coalitions of each coalition size and not on which coalitions within each coalition size that are included. To elaborate, consider $M = 4$ and $q = 3$, then $\mathcal{T} = \{\{1\}, \{2\}, \{1, 3\}\}$ and $\mathcal{T}^* = \{\{1\}, \{3\}, \{1, 2\}\}$ yields $P_{\mathcal{T}} = P_{\mathcal{T}^*}$ as both have two paired coalitions with size one and one with size two. Thus, we can reformulate the right sum in (17) to no longer sum over all sets of paired coalitions that contain q unique paired coalitions, but rather to sum over all ways to distribute the q paired coalitions among the coalition sizes and then multiply with the number of ways to do this. Specifically, we distribute q

indistinguishable objects into $\lfloor M/2 \rfloor$ distinguishable groups, i.e., the paired coalition sizes introduced in Section 3.2. Each group, namely a coalition size $|\mathcal{S}|$, can hold at most $N_{|\mathcal{S}|} = \binom{M}{|\mathcal{S}|}$ objects, for $|\mathcal{S}| \in \{1, 2, \dots, \lfloor M/2 \rfloor\}$. This is known as a *constrained integer partition problem*. Note that if M is even, then the coalition size $|\mathcal{S}| = \lfloor M/2 \rfloor$ becomes a special case where $N_{|\mathcal{S}|} = \binom{M}{|\mathcal{S}|}/2$ since $|\mathcal{S}| = |\bar{\mathcal{S}}|$.

Our generalized reformulation of (17) is therefore

$$\mathbb{E}[L] = 2 \sum_{q=0}^{\tilde{N}_{\mathcal{S}}-1} (-1)^{\tilde{N}_{\mathcal{S}}-1-q} \binom{2^{M-1}-1-q-1}{2^{M-1}-1-\tilde{N}_{\mathcal{S}}} \sum_{|\tilde{\mathcal{T}}|=q} \prod_{|\mathcal{S}|=1}^{\lfloor M/2 \rfloor} \binom{N_{|\mathcal{S}|}}{\tilde{\mathcal{T}}_{|\mathcal{S}|}} \frac{1}{1-P_{\tilde{\mathcal{T}}}}, \quad (18)$$

where $\tilde{\mathcal{T}}$ is an integer partition of q . We consider different orders to be different partitions as the coalition sizes are distinguishable. To elaborate, when $M = 4$, then the possible coalition sizes are $|\mathcal{S}| \in \{1, 2\}$, while $N_1 = \binom{4}{1} = 4$ and $N_2 = \binom{4}{2}/2 = 3$. When $q = 4$, then the possible partitions are $\tilde{\mathcal{T}} \in \{\{1, 3\}, \{2, 2\}, \{3, 1\}, \{4, 0\}\}$, where the orders $\{1, 3\}$ and $\{3, 1\}$ are treated as different partitions. For the partition $\tilde{\mathcal{T}} = \{2, 2\}$, we have $\binom{N_1}{\tilde{\mathcal{T}}_1} = \binom{4}{2} = 6$ ways to select the two paired coalitions of size one, while $\binom{N_2}{\tilde{\mathcal{T}}_2} = \binom{3}{2} = 3$. Thus, we have a total of $\prod_{|\mathcal{S}|=1}^{\lfloor M/2 \rfloor} \binom{N_{|\mathcal{S}|}}{\tilde{\mathcal{T}}_{|\mathcal{S}|}} = 6 \times 3 = 18$ coalition sets that yield the same $P_{\tilde{\mathcal{T}}}$ value.

To understand the importance of the group reformulation in (18), consider an example with $M = 10$ and $q = 255$. The right-most sum in (17) then contains $\binom{511}{255} \approx 2.36 \times 10^{152}$ terms, while the right-most sum in (18) contains “*merely*” 7 509 106 terms. That is a reduction by a factor of approximately 3.15×10^{145} . However, even with this reformulation, we cannot compute the exact expectations for $M > 10$ in a feasible time⁴. For $M > 10$, we simulate 1000 L values and use the empirical mean as an estimator, i.e., $\bar{L} = \frac{1}{1000} \sum_{l=1}^{1000} L_l \approx \mathbb{E}[L]$.

We insert (18) into (14) to obtain the weights used by the **paired cel-kernel** strategy in (7) when approximating the Shapley value explanations, that is,

$$w_{\mathcal{S}} \propto \frac{2p_{\mathcal{S}}}{1 - (1 - 2p_{\mathcal{S}})^{\mathbb{E}[L]/2}}. \quad (19)$$

For the sake of clarity, we stress that (19) does *not* yield $\mathbb{E}[\tilde{p}_{\mathcal{S}}]$ as (14) is non-linear. However, inserting $\mathbb{E}[L]$ will act as a proxy to $\mathbb{E}[\tilde{p}_{\mathcal{S}}]$, and in Figure 2, we illustrate that the difference is neglectable. There, the **paired cel-kernel** weights are illustrated by the dotted lines, while the $\mathbb{E}[\tilde{p}_{\mathcal{S}}]$ weights are given by the solid curves. The **paired cel-kernel** weights accurately follow the $\mathbb{E}[\tilde{p}_{\mathcal{S}}]$ weights and tend to the Shapley kernel weights when $N_{\mathcal{S}} \rightarrow 2^M$. We demonstrate the equal performance of the two versions in Appendix F. Note that we only include the weights for $|\mathcal{S}| \leq \lfloor M/2 \rfloor$ in Figure 2 as we defined \mathcal{S} to be the smaller one of \mathcal{S} and $\bar{\mathcal{S}}$ in Section 3.2. Additionally, the weights for the coalition sizes $|\mathcal{S}|$ (e.g., j) and $|\bar{\mathcal{S}}|$ (e.g., $M - j$) are equal due to the symmetry of the paired sampling. Furthermore, the weights are independent of the model and explicands and only depend on the number of features M . Thus, these weights can be precomputed, stored, and used when applicable.

3.7 Paired Imp C-Kernel

The **paired imp c-kernel** strategy extends the **paired c-kernel** strategy by including the most important paired coalitions, i.e., those with the largest Shapley kernel weights, first. This involves initially including coalitions \mathcal{S} with one feature together with their complements $\bar{\mathcal{S}}$ with $M - 1$ features, followed by coalitions with two features together with their complements with $M - 2$ features, and so on. We sample which coalitions to include in a paired manner for the coalition size where not all coalitions are included. That is, if $N_{\mathcal{S}}$ is even, both \mathcal{S} and its complement $\bar{\mathcal{S}}$ are included, while only \mathcal{S} is included when $N_{\mathcal{S}}$ is odd.

⁴For $M = 10$, it takes approximately 19 hours to compute (18) using 16 threads on an ARM Neoverse N1 with 512GB RAM. In contrast, simulating 1000 L values and computing their mean takes a few minutes using a single thread, with only minuscule differences in the results, see Figure 16 in Appendix C. Some of the long computation time can be attributed to the **gmp** package (Lucas et al. 2024), which is necessary to handle arbitrary precision arithmetic. The **integer** class in R cannot store large enough integers and the **numeric** class lacks sufficient precision, which leads to floating point errors that become significant when accumulated.

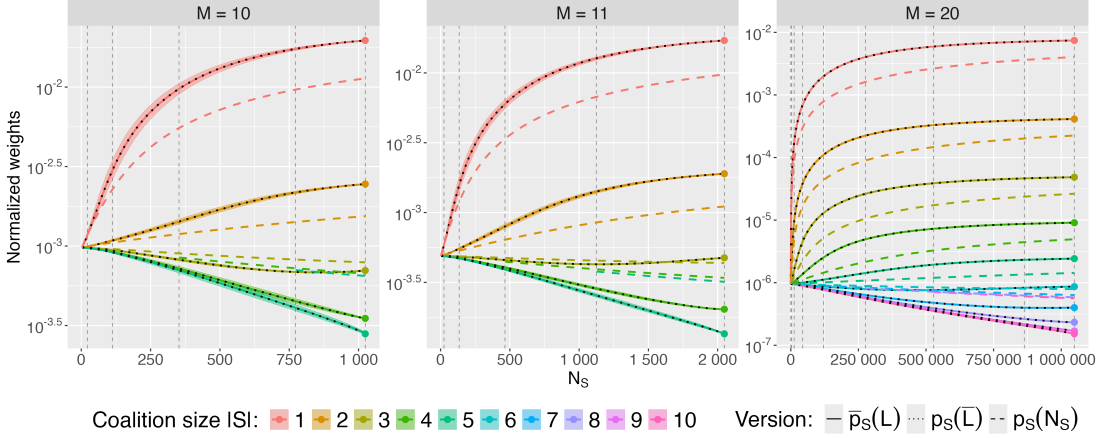


Figure 2: The normalized weights used by the **paired c-kernel**, **paired cel-kernel**, **paired imp c-kernel**, and **paired imp cel-kernel** strategies in (7) for $M \in \{10, 11, 17\}$. The dots represent the Shapley kernel weights and are provided in Table 2. **Dashed:** At the i th vertical dashed line, the **paired imp** strategies include all coalitions with size $|\mathcal{S}| \leq i$ and their complements. The dashed curves represent the weights used by the **paired imp c-kernel** strategy with sequence length $L = N_S$ for the different coalition sizes. The weights for coalition size $i + 1$ are only available to the right of the i th vertical dashed line and do not tend to the normalized Shapley kernel weights. **Solid:** We simulate 1000 coalition sequence lengths L for each N_S value, compute (14) for each L , and plot the mean $\bar{p}_S(L)$ values together with 95% empirical confidence bands. The bands represent the variability in the weights used by the **paired c-kernel** strategy, which is induced by L being stochastic. The variability is quite low, i.e., narrow bands, especially for large N_S values. The **paired average** weights (not included here) almost completely overlap the solid curves. **Dotted:** The dotted curves represent the weights used by the **paired cel-kernel** and **paired imp cel-kernel** strategies. Here we use the mean of the 1000 sequence lengths \bar{L} to compute (14). The $p_S(\bar{L})$ values almost perfectly match the $\bar{p}_S(L)$ values. For $M \leq 10$, we use the theoretical $\mathbb{E}[L]$ derived in (18) instead of \bar{L} .

M	$ \mathcal{S} = 1$	$ \mathcal{S} = 2$	$ \mathcal{S} = 3$	$ \mathcal{S} = 4$	$ \mathcal{S} = 5$	$ \mathcal{S} = 6$	$ \mathcal{S} = 7$	$ \mathcal{S} = 8$	$ \mathcal{S} = 9$	$ \mathcal{S} = 10$
10	1.96e-2	2.45e-3	7.01e-4	3.51e-4	2.81e-4	—	—	—	—	—
11	1.71e-2	1.90e-3	4.74e-4	2.03e-4	1.35e-4	—	—	—	—	—
20	7.42e-3	4.12e-4	4.85e-5	9.09e-6	2.42e-6	8.66e-7	4.00e-7	2.33e-7	1.70e-7	1.53e-7

Table 2: The normalized Shapley kernel weights p_S in (8) for different values of M and coalition sizes.

For clarity, consider an example with $M = 10$ and $N_S = 25$. The strategy first includes all size zero and one coalitions along with their paired complements, of which there are two and twenty coalitions, respectively. For the remaining three coalitions, we sample two coalitions uniformly (without replacement) from size-two coalitions, e.g., $\{1, 2\}$ and $\{5, 9\}$. We then include the paired complement of the first sampled coalition, $\{3, 4, 5, 6, 7, 8, 9, 10\}$, to reach the target of twenty-five coalitions. In Appendix E.3, we outline and discuss potential methods to include the coalitions based on pilot estimates of their importance instead of random sampling to improve the strategy.

The **paired imp c-kernel** strategy applies the Shapley kernel weight correction in (14) to obtain the weights w_S used in (7) when approximating Shapley values. However, the semi-deterministic

inclusion method means that $L = N_S$ and the corresponding weights are therefore given by

$$w_S \propto \frac{2p_S}{1 - (1 - 2p_S)^{N_S/2}}. \quad (20)$$

A consequence of the semi-deterministic inclusion is that the correction in (14) becomes invalid since it relies on the assumption that the sampling probability of coalition S is p_S . Therefore, (20) will not converge to the exact Shapley values when N_S approaches 2^M . This is illustrated by the dashed curves in Figure 2 not converging to the dots, which represent the Shapley kernel weights.

3.8 Paired Imp CEL-Kernel

The `paired imp cel-kernel` strategy modifies the `paired imp c-kernel` strategy by replacing $L = N_S$ in (20) with the expected value of L given in (18). That is, the modified weights are given by

$$w_S \propto \frac{2p_S}{1 - (1 - 2p_S)^{\mathbb{E}[L]/2}}. \quad (21)$$

This adjustment ensures that the Shapley value approximations obtained by the `paired imp cel-kernel` strategy converges to the exact Shapley values when N_S approaches 2^M , which is illustrated by the black dotted curves in Figure 2 converging to the normalized Shapley kernel weights in (8).

4 Numerical Simulation Studies

A major problem in evaluating explanation frameworks is that real-world data has no true Shapley value explanations. In this section, we consider two setups where we simulate Gaussian data for which we can compute the true/exact Shapley values ϕ using all 2^M coalitions. We then compare how close the approximated Shapley values $\phi_{\mathcal{D}}$ are ϕ using the different strategies and based on the coalitions in $\mathcal{D} \subset \mathcal{P}(\mathcal{M})$. This paper does not focus on estimating the contribution functions $v(S)$ but on strategies for selecting the coalitions \mathcal{S} . Thus, we compute the $v(S)$ once using the `gaussian` approach in the `shapr`-package (Sellereite and Jullum 2019) or analytical results, store them, and load the needed $v(S)$ values for the sampling strategies.

To elaborate, we generate the training observations and explicands from a multivariate Gaussian distribution $p(\mathbf{x}) = p(\mathbf{x}_S, \mathbf{x}_{\bar{S}}) = \mathcal{N}_M(\boldsymbol{\mu}, \boldsymbol{\Sigma})$, where $\boldsymbol{\mu} = [\boldsymbol{\mu}_S, \boldsymbol{\mu}_{\bar{S}}]^T$ and $\boldsymbol{\Sigma} = \begin{bmatrix} \boldsymbol{\Sigma}_{SS} & \boldsymbol{\Sigma}_{S\bar{S}} \\ \boldsymbol{\Sigma}_{\bar{S}S} & \boldsymbol{\Sigma}_{\bar{S}\bar{S}} \end{bmatrix}$. The conditional distribution is then $p(\mathbf{x}_{\bar{S}}|\mathbf{x}_S = \mathbf{x}_S^*) = \mathcal{N}_{|\bar{S}|}(\boldsymbol{\mu}_{\bar{S}|\mathcal{S}}, \boldsymbol{\Sigma}_{\bar{S}|\mathcal{S}})$, where $\boldsymbol{\mu}_{\bar{S}|\mathcal{S}} = \boldsymbol{\mu}_{\bar{S}} + \boldsymbol{\Sigma}_{\bar{S}S} \boldsymbol{\Sigma}_{SS}^{-1}(\mathbf{x}_S^* - \boldsymbol{\mu}_S)$ and $\boldsymbol{\Sigma}_{\bar{S}|\mathcal{S}} = \boldsymbol{\Sigma}_{\bar{S}\bar{S}} - \boldsymbol{\Sigma}_{\bar{S}S} \boldsymbol{\Sigma}_{SS}^{-1} \boldsymbol{\Sigma}_{S\bar{S}}$. The `gaussian` approach in `shapr` generate conditional samples $\mathbf{x}_{\bar{S}}^{(k)}$ from $p(\mathbf{x}_{\bar{S}}|\mathbf{x}_S = \mathbf{x}_S^*)$, for $k = 1, 2, \dots, K$ and $\mathcal{S} \in \mathcal{P}^*(\mathcal{M})$, and use them in (3) to accurately estimate the contribution functions. The parameters $\boldsymbol{\mu}$ and $\boldsymbol{\Sigma}$ are easily estimated using the sample mean and covariance matrix of the training data, respectively. However, we provide the true parameters to `shapr` to eliminate the uncertainty in estimating them and to obtain the true Shapley values.

We evaluate the performance of the sampling strategies by computing the averaged mean absolute error (MAE) between the exact (ϕ) and approximated ($\phi_{\mathcal{D}}$) Shapley values, averaged over B repetitions (different seeds), N_{explain} explicands, and M features. A similar criterion has been used in Redelmeier et al. (2020), Aas et al. (2021a,b), Olsen et al. (2022, 2024), and Olsen (2023). The MAE is given by

$$\text{MAE} = \overline{\text{MAE}}_B(\phi, \phi_{\mathcal{D}}) = \frac{1}{B} \sum_{b=1}^B \text{MAE}_b = \frac{1}{B} \sum_{b=1}^B \frac{1}{N_{\text{explain}}} \sum_{i=1}^{N_{\text{explain}}} \frac{1}{M} \sum_{j=1}^M |\phi_{i,j} - \phi_{\mathcal{D}_b, i,j}|. \quad (22)$$

To speed up the computations, we recycle the sampled coalitions for strategies using the same sampling procedure. That is, the `paired`, `paired average`, `paired kernel`, `paired c-kernel`, and `paired cel-kernel` strategies all use the same sampling procedure before weighing the coalitions differently. Furthermore, the `paired imp c-kernel` and `paired imp cel-kernel` strategies also share their sampling procedure, while the `unique` strategy has a separate sampling procedure. To mitigate

a separate sampling step for each increasing value of N_S , we sample a sequence/set of coalitions \mathcal{D} until all 2^M coalitions are included and keep track of at which index the sequence contains N_S unique coalitions. We can then efficiently “sample” the set \mathcal{D} with N_S unique coalitions by extracting the coalitions up to this index from the sequence. This is done for each of the B repetitions.

Remark: The sampling step is more expensive for the first six strategies in Section 3 due to the repeated sampling with replacements. More precisely, the sampling procedure is time-consuming when $N_S \approx 2^M$ and M is large as the probability of sampling one of the $N_S - |\mathcal{D}|$ remaining unique coalitions is minuscule and takes many iterations. For the **paired** sampling procedure in the $M = 20$ -dimensional setting in Section 4.2, we sample on average $L = 80\,738\,405$ coalitions before we have $2^M = 1\,048\,576$ unique coalitions. In Figure 15 in Appendix C, we plot the average L and $E[L]$ as functions of N_S for different values of M . In contrast, the sampling procedure used by the **paired imp c-kernel** and **paired imp cel-kernel** strategies is almost instantaneous due to direct sampling without replacement. For the **paired kernel** and **paired cel-kernel** strategies, which do not use the sampling frequencies or sequence length, we can speed up the sampling by listing all possible coalitions and conducting weighted sampling without replacements with p_S (8) as sampling probabilities. However, listing all coalitions is impossible if M is too large. When the coalitions in \mathcal{D} are determined, the computation of the approximated Shapley values in (7) is computed in the order of seconds as we load the stored $v(S)$ values and do not have to compute them. In general, the computation of the contribution functions is often the most computationally demanding part (Olsen et al. 2024).

4.1 XGBoost Model

We let $M = 10$ and $N_{\text{train}} = N_{\text{explain}} = 1000$. We generate the data according to a multivariate Gaussian distribution $\mathbf{x} \sim \mathcal{N}_M(\mathbf{0}, \Sigma)$, where Σ is the equi-correlation matrix⁵. That is, 1 on the diagonal and $\rho \in \{0, 0.2, 0.5, 0.9\}$ off-diagonal, where one value of ρ is used in each experiment. We generate a response according to $y = 2 + 10X_1 + 0.25X_2 - 3X_3 - X_4 + 1.5X_5 - 0.5X_6 + 10X_7 + 1.25X_8 + 1.5X_9 - 2X_{10} + X_1X_2 - 2X_3X_5 + 2X_4X_8 - 3X_9X_{10} + 3X_1X_3X_7 - X_2X_6X_8 - 2X_3X_8X_{10} + 4X_1X_4X_7X_9$.

We fit a cross-validated **xgboost** model (Chen et al. 2015) to this regression problem to act as the predictive model f . To obtain the true/exact Shapley values ϕ , we use Monte Carlo integration with $K = 5000$ Monte Carlo samples for each coalition and explicand. This is done using the **gaussian** approach in the **shapr**-package and the true Shapley values are illustrated with sina plots in Appendix D. We repeat the sampling strategies $B = 500$ times as they are stochastic.

In Figure 3, we plot the MAE curves for the different strategies and dependence levels as a function of N_S . We also include 95% empirical confidence bands to illustrate the uncertainty in the 500 repeated experiments. Our novel strategies outperform the other established **unique** and **paired** sampling strategies for all dependence levels. The state-of-the-art **paired** strategy outperforms the **unique** strategy. Still, it is (almost) uniformly outperformed by our **paired average**, **paired c-kernel**, and **paired cel-kernel** strategies by a significant margin. This means that the simple weight-stabilizing technique in the **paired average** strategy lowers the MAE values. However, the **paired c-kernel** strategy, which uses the corrected Shapley kernel weights instead of the stabilized sampling frequencies, gives additional improvements. Directly using the (uncorrected) Shapley kernel weights, as in the **paired kernel** strategy, yields poor approximations unless N_S is close to 2^M . Finally, the **paired cel-kernel** strategy further improves the **paired c-kernel** strategy by lowering the MAE scores by a small margin.

In general, our novel strategies improve the most upon the established **paired** strategy for the larger dependence levels, and the difference in the MAE scores between the strategies increases when N_S increases. The **paired c-kernel** and **paired cel-kernel** strategies produce slightly more accurate Shapley value approximations than the **paired average** strategy. However, the difference is mainly noticeable for larger values of N_S . We discuss this difference more at the end of the section.

The **paired imp c-kernel** strategy performs very well for low values of N_S . However, after including all coalitions up to size 3 (and their complements), the precision of the approximated Shapley values deteriorates, and the MAE scores drastically increase. We do not have an explicit explanation

⁵We obtain nearly identical results when $\Sigma_{i,j} = \rho^{|i-j|}$.

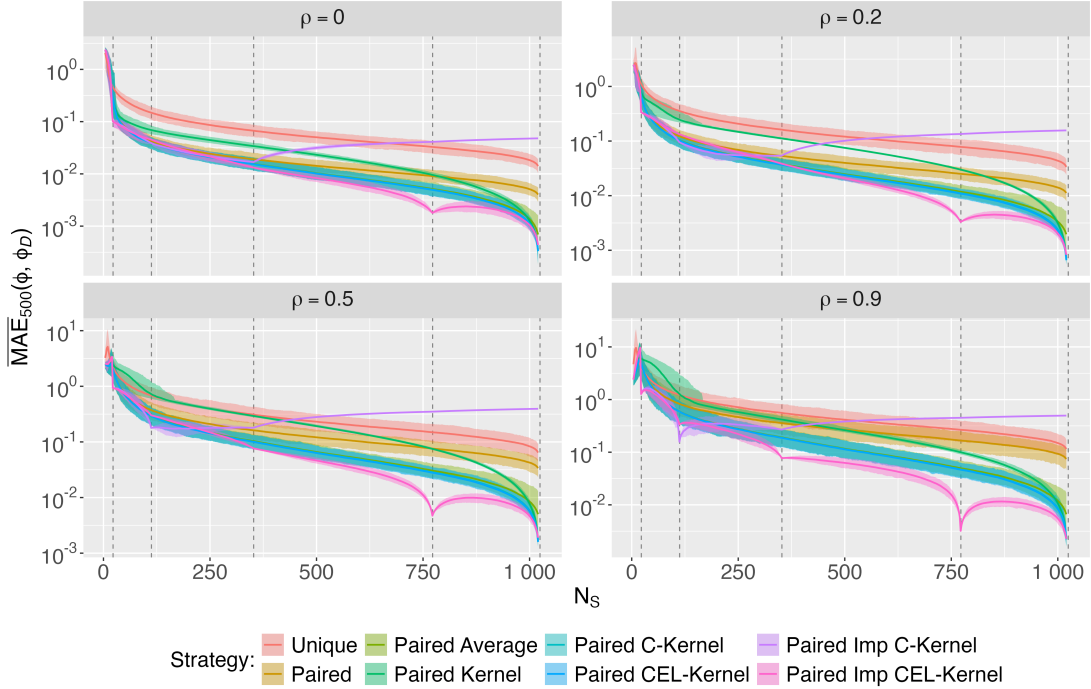


Figure 3: XGBoost experiment: $\text{MAE} = \overline{\text{MAE}}_{500}(\phi, \phi_{\mathcal{D}})$ for different number of coalitions N_S and dependencies levels ρ on log-scale together with 95% confidence bands. At the i th vertical dashed line, the **paired imp** strategies include all coalitions with size $|\mathcal{S}| \leq i$ and their complements.

for the location of the dip, and we include it as a part of further research in Section 6. However, the increase in the MAE values when N_S tends to 2^M is as expected and explained in Section 3.7. This behavior is corrected by the **paired imp cel-kernel** strategy.

The **paired imp cel-kernel** strategy is the best strategy in the simulation study and is on par with or outperforms all other strategies. It is only marginally outperformed by the **paired average** and **paired c-kernel** strategies for low values of N_S . Note that the **paired imp cel-kernel** strategy tends to obtain increased precision when it includes all coalitions of the same size, i.e., the dips in the curves at the dashed vertical lines in Figure 3. The dips are very evident for higher dependence levels. The **paired kernel** strategy outperforms the **paired** strategy for larger values of N_S . Still, it is never at the same precision level as the **paired average**, **paired c-kernel**, **paired cel-kernel**, and **paired imp cel-kernel** strategies.

The MAE values should be interpreted together with f to better understand the scale of the errors. Recall the efficiency axiom which states that $f(\mathbf{x}^*) = \phi_0 + \sum_{j=1}^M \phi_j^*$. That is, the Shapley values explain the difference between ϕ_0 and the predicted response $f(\mathbf{x}^*)$ for different explicands \mathbf{x}^* . In Figure 4, we plot histograms of the $f(\mathbf{x}^*)$ values together with the corresponding ϕ_0 values for the four dependence levels. If the difference between ϕ_0 and $f(\mathbf{x}^*)$ is small, then the Shapley values are often small too; we illustrate this for the real-world data set in Section 5. Thus, obtaining a low absolute error is easier for explicands with a predicted response closer to ϕ_0 .

In the simulation studies, we have that $\frac{1}{N_{\text{explain}}} \sum_{i=1}^{N_{\text{explain}}} |\phi_0 - f(\mathbf{x}^*)|$ equals 11.54, 12.27, 13.02, 15.98 for the four dependence levels $\rho \in \{0, 0.2, 0.5, 0.9\}$, respectively. This means that, on average, each of the ten absolute Shapley values are 1.154, 1.227, 1.302, and 1.598, respectively. Thus, we consider an MAE between 10^{-1} and 10^{-2} to yield satisfactory accurate approximated Shapley values. Which corresponds to an N_S around 300 to 500 in the different setups for the **paired average**, **paired**

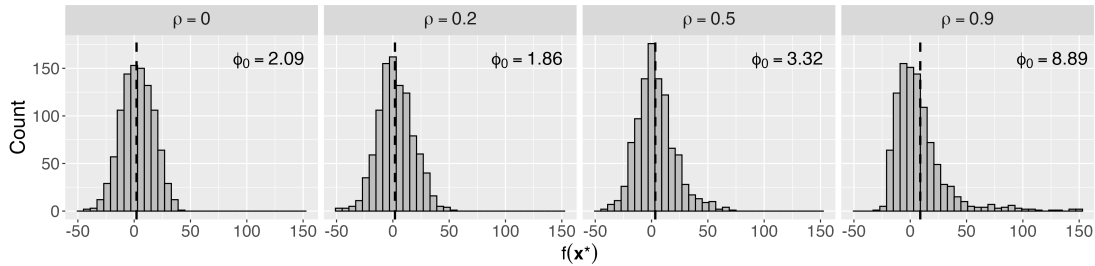


Figure 4: XGBoost experiment: histograms of the predicted responses $f(\mathbf{x}^*)$ for the 1000 explicands together with $\phi_0 = \mathbb{E}[f(\mathbf{x})] = \bar{y}_{\text{train}}$ for each dependence level.

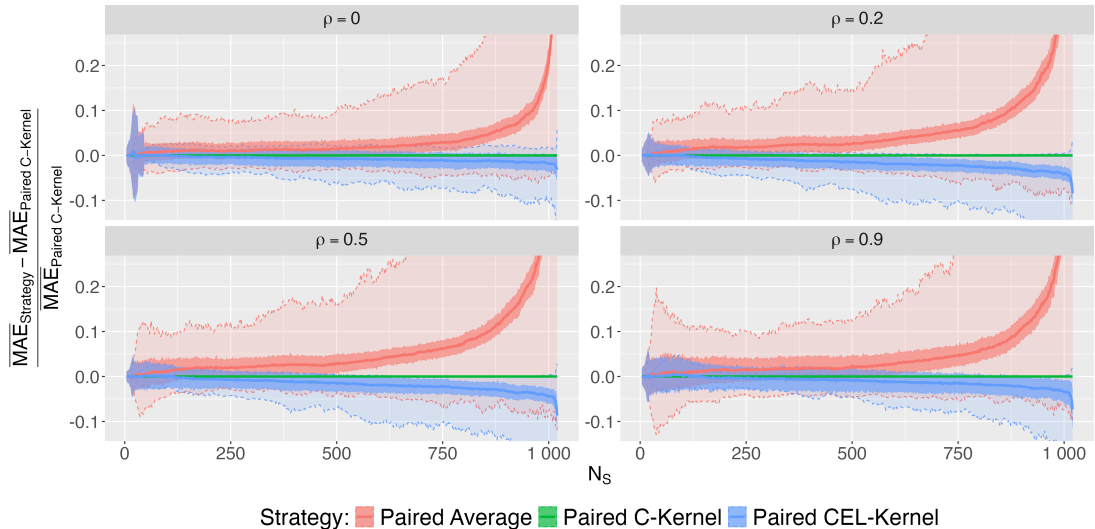


Figure 5: XGBoost experiment: the relative $\overline{\text{MAE}}_{500}(\phi, \phi_{\mathcal{D}})$ difference between the strategies with **paired c-kernel** as the reference. The solid and dashed confidence bands are 95% confidence bands for the relative $\overline{\text{MAE}}_{500}$ and MAE_b differences, respectively. Lower values are better.

c-kernel, **paired cel-kernel** and **paired imp cel-kernel** strategies. In Figure 6, we illustrate the reduction in N_S when using the **paired c-kernel** strategy to achieve the same MAE scores as the **unique** and **paired** strategies. In practice, where we do not have access to ϕ , it is more applicable to gradually increase N_S until $\phi_{\mathcal{D}}$ obtains some convergence criterion; see Covert and Lee (2021).

In Figure 5, we plot the relative difference in $\text{MAE} = \overline{\text{MAE}}_{500}(\phi, \phi_{\mathcal{D}})$ values obtained by the **paired average**, **paired c-kernel**, and **paired cel-kernel** strategies when using the **paired c-kernel** strategies as the reference. The relative difference is included to more easily distinguish the performance of these strategies, as their confidence bands in Figure 3 overlap and are difficult to separate. In Figure 5, we observe that, on average, the **paired cel-kernel** strategy obtains a lower relative error compared to **paired c-kernel**, whereas the **paired average** obtains a higher relative error. The solid confidence bands indicate the uncertainty around $\overline{\text{MAE}}_{500}$, while the dashed confidence bands indicate the uncertainty between the B repetitions. The solid confidence bands show that the average relative error is significantly different between the strategies, especially when N_S increases. However, the somewhat overlapping dashed confidence bands tell us that the order of the strategies can be different for some of the B repetitions. In practice, the absolute difference in the MAE scores between these strategies is minuscule and is unlikely to have any consequential practical implications.

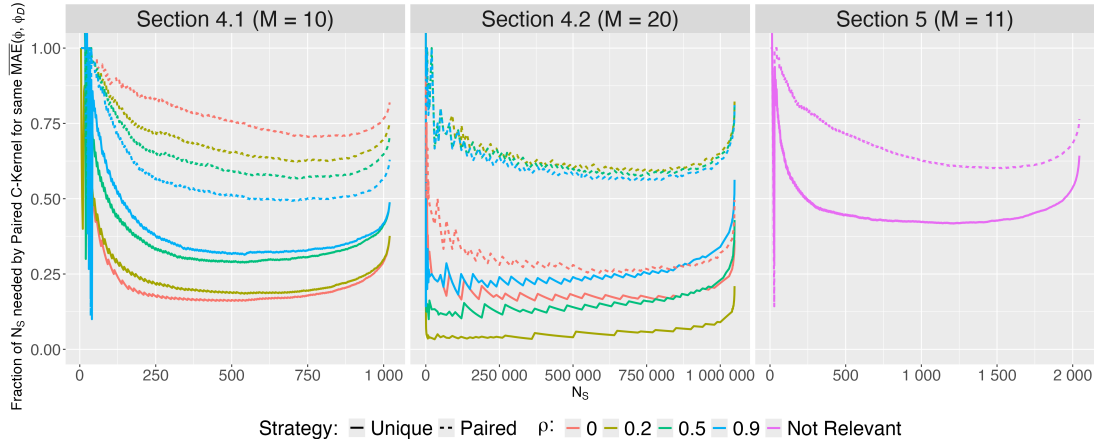


Figure 6: Illustration of the reduction in the number of unique coalitions N_S needed by the **paired c-kernel** strategy to obtain the same precision, i.e., the same $\overline{\text{MAE}}(\phi, \phi_D)$ value, as the **unique** and **paired** strategies. For the experiment in Section 5, we see that when $N_S = 1000$, the **paired c-kernel** strategy obtains the same precision as the **paired** strategy using only $0.625 \times 1000 = 625$ coalitions, while only 400 coalitions are needed when compared to the **unique** strategy. For the simulation studies in Sections 4.1 and 4.2, the dependence level affects the reduction. When comparing the **unique** and **paired c-kernel** strategies, we see that the reduction is largest for independent features and decreases with increasing dependencies. Conversely, when comparing the **paired** and **paired c-kernel** strategies, the reduction is most significant for high dependence levels.

4.2 Linear Regression Model

In the second simulation study, we investigate a larger dimensional setup. However, we are limited by the computational complexity of the true Shapley values growing exponentially with the number of features. Thus, we settle on an $M = 20$ -dimensional Gaussian data setup with a linear model as the predictive model f , as we can then obtain analytical expressions for the contribution function (Aas et al. 2021a, Appendix B.2). More precisely, the contribution function in (2) for linear models with dependent features simplifies to $v(\mathcal{S}) = f(\mathbf{x}_{\bar{\mathcal{S}}} = \boldsymbol{\mu}_{\bar{\mathcal{S}}}, \mathbf{x}_{\mathcal{S}} = \mathbf{x}_{\mathcal{S}}^*)$, where $\boldsymbol{\mu}_{\bar{\mathcal{S}}} = \mathbb{E}[\mathbf{x}_{\bar{\mathcal{S}}}] = \boldsymbol{\mu}_{\bar{\mathcal{S}}} + \boldsymbol{\Sigma}_{\bar{\mathcal{S}}\mathcal{S}} \boldsymbol{\Sigma}_{\mathcal{S}\mathcal{S}}^{-1}(\mathbf{x}_{\mathcal{S}}^* - \boldsymbol{\mu}_{\mathcal{S}})$ for Gaussian data. This allows us to avoid time-consuming simulations needed in the Monte Carlo integration procedure in (3) when computing the contribution function values $v(\mathcal{S})$ for the $2^M = 1\,048\,576$ different coalitions and N_{explain} explicands.

We generate $N_{\text{train}} = 1000$ training observations and $N_{\text{explain}} = 250$ explicands according to the Gaussian distribution $\mathbf{x} \sim \mathcal{N}_M(\mathbf{0}, \boldsymbol{\Sigma}_\rho)$, where $\boldsymbol{\Sigma}_\rho = \text{diag}(B_3^\rho, B_4^\rho, B_3^\rho, B_5^\rho, B_2^\rho, B_2^\rho, B_1^\rho)$ is a block diagonal matrix. Here B_j^ρ is an equi-correlation matrix of dimension $j \times j$ and $\rho \in \{0, 0.2, 0.5, 0.9\}$. We generate the responses according to $\mathbf{y} = \mathbf{X}\boldsymbol{\beta}$, where $\boldsymbol{\beta} = [2, 1, 0.25, -3, -1, 1.5, -0.5, 0.75, 1.25, 1.5, -2, 3, -1, -5, 4, -10, 2, 5, -0.5, -1, -2]$ and the first value is the intercept. We fit a linear model to the data and repeat the sampling strategies $B = 150$ times.

In Figure 7, we plot the MAE curves for each strategy together with 95% empirical confidence bands for the different dependence levels as a function of N_S . We do not focus on the $\rho = 0$ setting as it is a trivial case where the Shapley values are explicitly given by $\phi_j = \beta_j(x_j^* - \mathbb{E}[x_j])$, for $j = 1, 2, \dots, M$ (Aas et al. 2021a, Appendix B.1). Nevertheless, note that the **paired imp c-kernel** and **paired imp cel-kernel** strategies obtain near machine-error precise estimates when all coalitions in each coalition size are included and when all coalitions of size one through nine are included.

For all dependence levels, we see that our novel strategies outperform the established **unique** and **paired** strategies by a significant margin. The **paired average**, **paired c-kernel**, and **paired cel-kernel** strategies perform almost identically as their curves and confidence bands almost perfectly

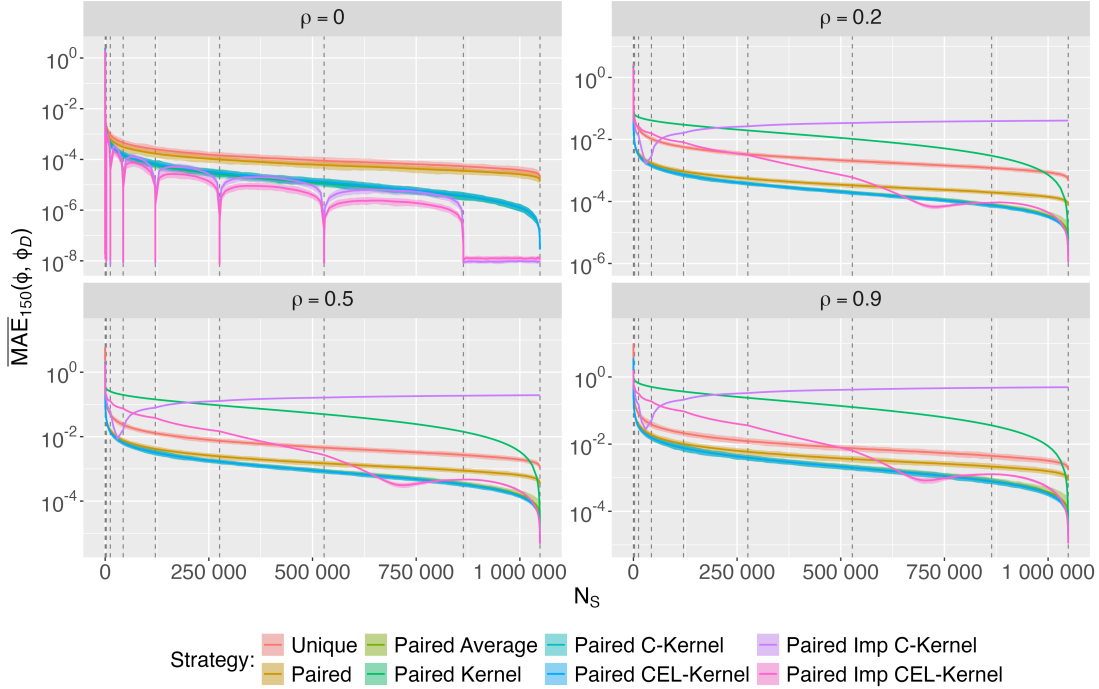


Figure 7: Linear experiment: $\text{MAE} = \overline{\text{MAE}}_{150}(\phi, \phi_D)$ curves for each strategy and dependence level ρ on log-scale together with 95% confidence bands, which are very narrow. At the i th vertical dashed line, the **paired imp** strategies include all coalitions with size $|\mathcal{S}| \leq i$ and their complements.

overlap, but the latter two obtain a marginally lower MAE for large values of N_S . We discuss this difference more at the end of the section. The **paired kernel** strategy is the worst strategy up to $N_S \leq 200\,000$, which is the region of the most interest. Except for $\rho = 0$, where it performs nearly identically to the **paired average**, **paired c-kernel**, and **paired cel-kernel** strategies. For $N_S \geq 200\,000$, the **paired imp c-kernel** strategy performs the worst, which is expected due to the incorrect weighting of coalitions. The **paired imp cel-kernel** strategy is the best when $N_S \in [650\,000, 750\,000]$, but it is significantly outperformed by the **paired average**, **paired c-kernel**, and **paired cel-kernel** strategies for lower values of N_S . Furthermore, we see no dips in the MAE curves for the **paired imp cel-kernel** strategy at the vertical dashed lines when $\rho > 0$.

In Figure 8, we plot histograms of the $f(\mathbf{x}^*)$ values together with the corresponding ϕ_0 values for the four dependence levels. Here the values of $\frac{1}{N_{\text{explain}}} \sum_{i=1}^{N_{\text{explain}}} |\phi_0 - f(\mathbf{x}^*)|$ equals 15.23, 14.89, 14.56, and 14.62, respectively. Which yields an average of 0.76, 0.74, 0.73, and 0.73 per Shapley value. Thus, we consider an MAE between 10^{-2} and $10^{-2.5}$ to give satisfactory accurate approximated Shapley values. Which corresponds to an N_S around 2000 to 300 000 in the different setups for the **paired average**, **paired c-kernel**, and **paired cel-kernel** strategies. Note that the number of coalitions N_S needed for this precision level increases when the dependence increases.

In Figure 9, we plot the relative difference in the MAE scores to illustrate that there are differences in the MAE scores for the **paired average**, **paired c-kernel**, and **paired cel-kernel** strategies, except for $\rho = 0$. From the solid confidence bands, which showcase the uncertainty around $\overline{\text{MAE}}_{500}$, we see that the **paired average** strategy is outperformed by the **paired c-kernel** strategy on average. This is especially evident for large values of N_S . While the **paired c-kernel** strategy is outperformed by the **paired cel-kernel** strategy on average. Based on the overlapping dashed confidence bands, which showcase the uncertainty between the B repetitions, we see that the order of the strategies can

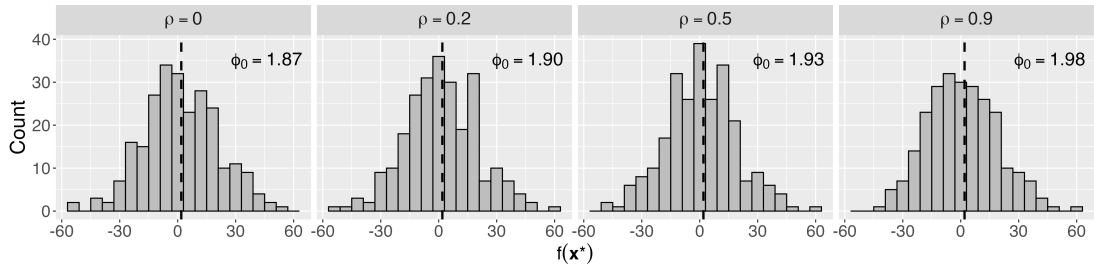


Figure 8: Linear experiment: histograms of the predicted responses $f(\mathbf{x}^*)$ for the 250 explicands together with $\phi_0 = \mathbb{E}[f(\mathbf{x})] = \bar{y}_{\text{train}}$ for each dependence level.

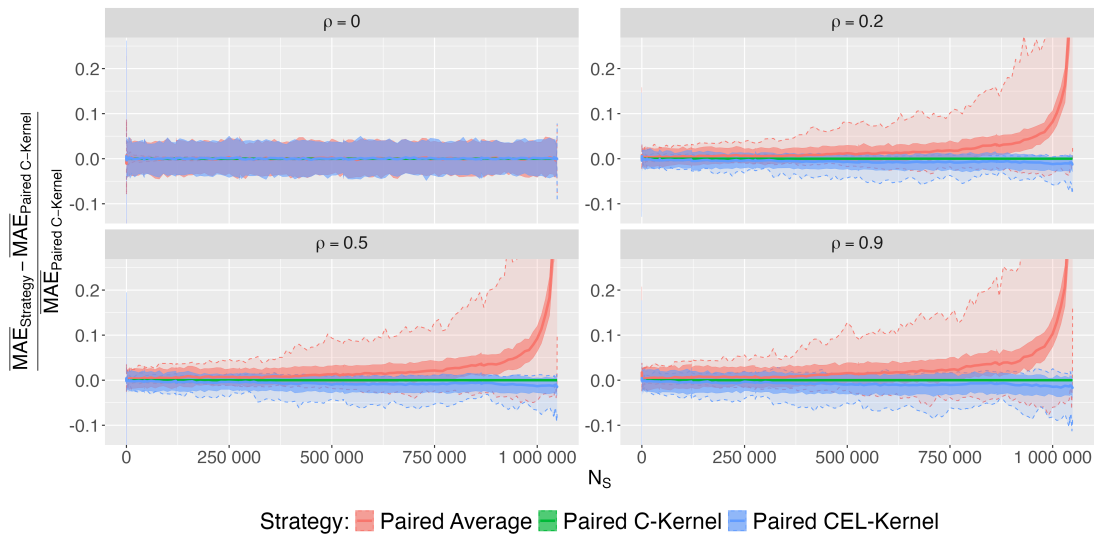


Figure 9: Linear experiment: the relative $\overline{\text{MAE}}_{150}(\phi, \phi_{\mathcal{D}})$ difference between the strategies with **paired c-kernel** as the reference. The solid and dashed confidence bands are 95% confidence bands for the relative $\overline{\text{MAE}}_{150}$ and MAE_b differences, respectively. Lower values are better.

change for some repetitions. However, we want to stress that the difference in the MAE values for the simple **paired c-kernel** and more complex **paired cel-kernel** strategies is minuscule and would most likely not affect a practitioner, i.e., the simple **paired c-kernel** strategy is sufficient in practice.

We obtain similar results to those in Figure 7 for other linear simulation experiments not included in this paper with $M \in \{10, 12, 14, 17, 20\}$ and different coefficient values and correlation matrices. The lack of dips at the vertical dashed lines in Figure 7, which we observed in Figure 3, are not an artifact of the equi-correlation matrix as they do not appear when we replace the block equi-correlation matrix with the full equi-correlation matrix. However, the gap between the **paired** strategy and the **paired average**, **paired c-kernel**, and **paired cel-kernel** strategies further increases and the dip in the MAE value for the **paired imp cel-kernel** strategy, which is stable at around $N_S = 700\,000$ in Figure 7, moves gradually from 600 000 to 400 000 when increasing ρ from 0.2 to 0.9.

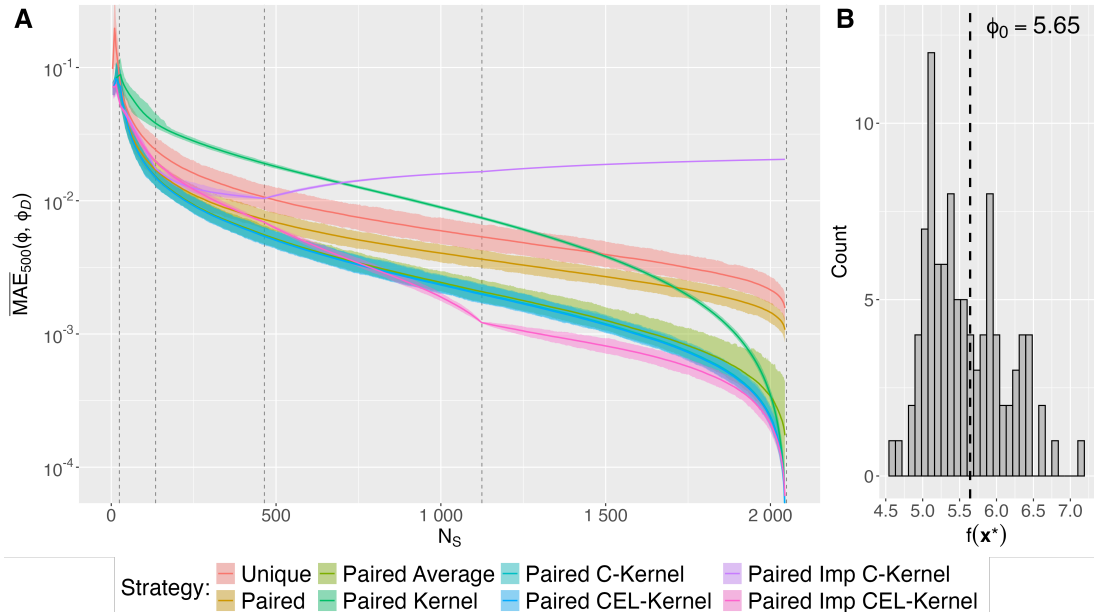


Figure 10: Red Wine experiment: **A**) The $\text{MAE} = \overline{\text{MAE}}_{500}(\phi, \phi_{\mathcal{D}})$ values with 95% confidence bands for different values of N_S on log-scale. **B**) Histogram of the predicted responses $f(\mathbf{x}^*)$ for the 99 explicands together with $\phi_0 = \mathbb{E}[f(\mathbf{x})] = \bar{y}_{\text{train}}$.

5 Real-World Data Experiments

We consider the Red Wine data set from the UCI Machine Learning Repository to evaluate the sampling strategies on real non-Gaussian data. We fit a cross-validated random forest model⁶ to act as the predictive model. We compute the Shapley values ϕ using the `random forest separate regression` approach in the `shapr` package⁷. Olsen et al. (2024) determined this approach to yield the most precise Shapley values for this data set and predictive model. The approach estimates (2) by a random forest model with default hyperparameter values: `trees = 500`, `mtry = 3`, and `min.node.size = 5`. We compare these Shapley values ϕ using all 2^M coalitions with the approximated Shapley values $\phi_{\mathcal{D}}$ obtained by using only $N_S = |\mathcal{D}|$ unique coalitions determined by the different sampling strategies.

The Red Wine data set contains information about variants of the Portuguese Vinho Verde wine (Cortez et al. 2009). The response is a `quality` value between 0 and 10, while the $M = 11$ continuous features are based on physicochemical tests: `fixed acidity`, `volatile acidity`, `citric acid`, `residual sugar`, `chlorides`, `free sulfur dioxide`, `total sulfur dioxide`, `density`, `pH`, `sulphates`, and `alcohol`. For the Red Wine data set, most scatter plots and marginal density functions display structures and marginals far from the Gaussian distribution, as most of the marginals are right-skewed (Olsen et al. 2024, Figure S10). Many features have no to moderate correlation, with a mean absolute correlation of 0.20, while the largest correlation in absolute value is 0.683 between `pH` and `fix.acid`. The data set contains 1599 wines, and we split it into a training (1500) and a test (99) data set.

In Figure 10, we display the $\text{MAE} = \overline{\text{MAE}}_{500}(\phi, \phi_{\mathcal{D}})$ values with 95% empirical confidence bands. The results are similar to those we obtained for the simulation studies in Section 4. The best strategy for a low to medium number of coalitions, i.e., $N_S \leq 750$, is any of the `paired average`, `paired c-kernel`, `paired cel-kernel` strategies. These strategies obtain nearly identical MAE scores and significantly outperform the `unique` and `paired` strategies for all values of N_S . The `paired imp`

⁶A `ranger` model (Wright and Ziegler 2017) with `trees = 200`, `mtry = 4`, and `min.node.size = 3`.

⁷See the regression vignette for an introduction to the `random forest separate regression` approach.

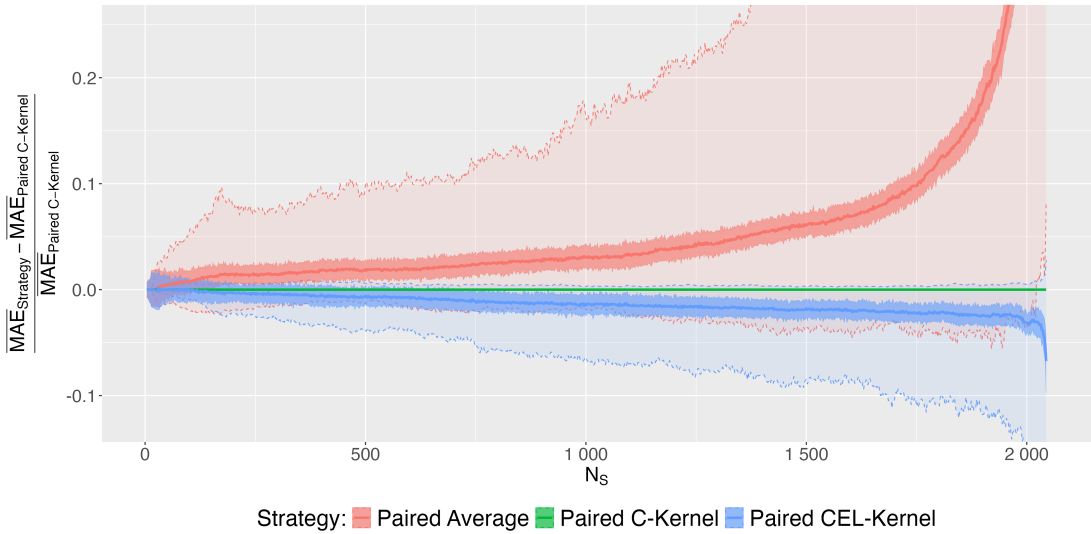


Figure 11: Red Wine experiment: the relative $\overline{\text{MAE}}_{500}(\phi, \phi_{\mathcal{D}})$ difference between the strategies with **paired c-kernel** as the reference. The solid and dashed confidence bands are 95% confidence bands for the relative $\overline{\text{MAE}}_{500}$ and MAE_b differences, respectively. Lower values are better.

cel-kernel strategy is the best strategy for $N_S \geq 750$, and it exhibits a dip in the MAE value when including all coalitions of size four and less.

The **paired kernel** strategy is the worst strategy for $N_S < 700$, but it becomes more precise as N_S increases and outperforms **paired average** when $N_S > 2000$. However, at that level, it would be reasonable to use all $2^{11} = 2048$ coalitions instead and omit the approximation step. Furthermore, it never catches up with the corrected versions, i.e., **paired c-kernel** and **paired cel-kernel**. The **paired imp c-kernel** strategy is the worst strategy for $N_S \geq 700$. As in Section 4.1, we see that the strategy’s performance drastically decline when it includes coalition sizes larger than three.

As stated in Section 4, the MAE should be interpreted together with the $f(\mathbf{x})$ to obtain a proper understanding of the scale of the errors. If the difference between $\phi_0 = 5.65$ and $f(\mathbf{x}^*)$ is small, then the Shapley values are often small too. See explicand four in Figure 12 with $f(\mathbf{x}^*) = 5.7$, where all but one Shapley value is less than 0.05 in absolute value. Thus, obtaining a low absolute error is easier for explicands with a predicted response closer to ϕ_0 . We have that $\frac{1}{N_{\text{explain}}} \sum_{i=1}^{N_{\text{explain}}} |\phi_0 - f(\mathbf{x}^*)| = 0.43947$, which means that the 11 Shapley values move the ϕ_0 value by 0.44, or 0.04 per Shapley value, on average. We consider an MAE of $10^{-2.5} \approx 0.0032$ and 10^{-3} to be to be low and very low, respectively. For the former, the **paired average**, **paired c-kernel**, **paired cel-kernel**, and **paired imp cel-kernel** strategies archive this for $N_S \approx 800$. For the very low MAE value, the **paired imp cel-kernel** strategy archives this at N_S around 1100, while the others achieve this around 1600. The **unique** and **paired** strategies never archive this precision level.

In Figure 12, we compare the approximated Shapley values $\phi_{\mathcal{D}}$ computed by the **paired c-kernel** strategy with the Shapley values ϕ using all coalitions for six explicands with increasing predicted responses. We see that the magnitude of the Shapley values is larger for predictions further away from ϕ_0 and the approximated Shapley values are close to the exact values for N_S larger than 100 to 200.

In Figure 11, we plot the relative difference between the **paired average**, **paired c-kernel**, **paired cel-kernel** strategies to demonstrate that there is a difference in the MAE = $\overline{\text{MAE}}_{500}(\phi, \phi_{\mathcal{D}})$ scores, even though it is small. We see that, on average, **paired cel-kernel** outperforms **paired c-kernel**, which again outperforms **paired average** by a significant margin based on the non-overlapping solid confidence bands. However, for a single repetition b , the order of the strategies can be different as the dashed confidence bands overlap.

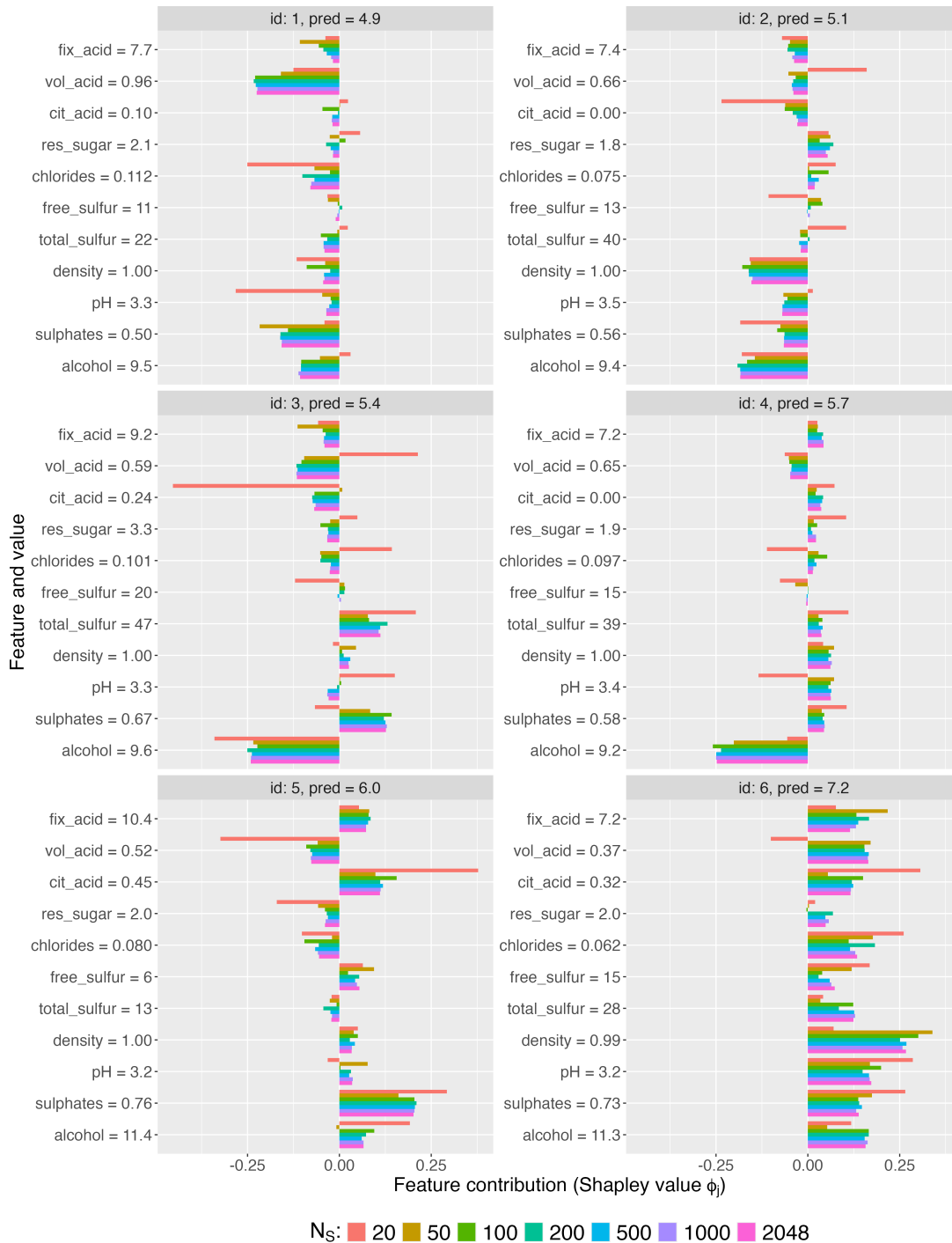


Figure 12: Red Wine experiment: comparing the Shapley values ϕ , obtained using all 2048 coalitions, with the approximated Shapley values $\phi_{\mathcal{D}}$ obtained by the simple paired c-kernel strategy when increasing the number of unique coalitions N_S in the subset \mathcal{D} . The approximated Shapley values are close to the exact values when N_S larger than 100 to 200.

6 Conclusion and Further Work

A major drawback of the Shapley value explanation framework is its computational complexity, which grows exponentially with the number of features. The `KernelSHAP` approximation framework addresses this by approximating Shapley values as the solution to a weighted least squares problem using a sampled subset \mathcal{D} of the 2^M coalitions (Lundberg and Lee 2017). We introduce several novel strategies for selecting \mathcal{D} and weighing its N_S unique elements. Our `paired average` strategy extends the state-of-the-art `paired` strategy (Covert and Lee 2021) within the `KernelSHAP` framework by pairing not only the sampling frequencies of paired coalitions but also within the different coalition sizes. By averaging the sampling frequencies within each coalition size, we ensure faster and more stable convergence to the Shapley kernel weights. The novel `paired c-kernel` strategy directly utilizes the Shapley kernel weights but corrects them based on the sampled subset. While the `paired cel-kernel` strategy takes the expectation over the subset to remove the variance and produce deterministic weights. The `paired imp c-kernel` and `paired imp cel-kernel` strategies determine the subset of coalitions in a semi-deterministic way by including the most important coalitions first.

Through simulation studies and real-world data examples, we demonstrate that our strategies lead to uniformly more accurate Shapley value explanations using fewer coalitions than competing strategies. More specifically, the `paired` strategy is consistently outperformed by the `paired average` strategy, which in turn is outperformed by the `paired c-kernel` strategy. The more complex `paired cel-kernel` strategy outperforms the `paired c-kernel` strategy. However, the difference is negligible and unlikely to affect practical applications. The `paired imp c-kernel` and `paired imp cel-kernel` strategies, especially the latter, produce the most accurate Shapley value approximations of all strategies within certain ranges of N_S values, but it is often significantly worse outside these regions. Identifying these regions in advance is challenging. Based on our simulation studies and experiments, we recommend the `paired c-kernel` strategy for its simplicity and consistently high accuracy.

We identify four potential areas for further research. First, we can develop a deeper understanding of when and why the `paired imp c-kernel` and `paired imp cel-kernel` strategies perform well. This analysis should explore whether certain data properties or model characteristics influence their effectiveness. Second, we may extend and enhance our strategies by guiding the sampling of coalitions toward more informative coalitions using pilot estimates. We outline preliminary work on this idea in Appendix E. Third, we can theoretically prove the variance reduction properties of, e.g., the `paired average` and `paired c-kernel` strategies, similar to the proof provided by Covert and Lee (2021, Theorem 1.) for the `paired` strategy. Additionally, investigate whether these weighting schemes are optimal or if better alternatives can be discovered. In a smaller-dimensional setup, one can consider brute force to see if we can find another set of better weights. We can then use the findings to build intuition and extend it to higher dimensions and theoretical results. Fourth, we can compare our strategies with those proposed for other Shapley value approximation frameworks beyond `KernelSHAP`. For instance, strategies for the *random order value* formulation have been proposed by Mitchell et al. (2022), Campen et al. (2018), Illés and Kerényi (2019), and Castro et al. (2017). Notably, Mitchell et al. (2022) find that a paired sampling strategy achieves near-best convergence compared to more complex alternatives. Additionally, comparisons could include the projected gradient descent strategy by Simon and Vincent (2020) or the *amortized explanation model* by Jethani et al. (2021), which uses a neural network to directly output approximated Shapley values for classification problems.

The main computational burden of approximating Shapley values lies in estimating the contribution function values $v(\mathcal{S})$ rather than sampling and determining the weights of the coalitions \mathcal{S} . Therefore, our proposed strategies, which reduce the number of unique coalitions N_S while maintaining the accuracy of the approximated Shapley values, are very computationally beneficial. For example, we approximately halve the computation cost and time when we halve the number of coalitions. In Figure 6, we illustrate the reduction in N_S when using the `paired c-kernel` strategy to achieve the same accuracy as the `unique` and `paired` strategies. The `paired c-kernel` strategy reduces the required number of coalitions by 50% to 95% compared to the `unique` strategy and by 25% to 50% compared to the `paired` strategy, depending on N_S and the dependence level between the features. This substantial decrease significantly lowers the computational cost and time for Shapley value explanations, making them more feasible in practical applications.

Acknowledgments

The Norwegian Research Council supported this research through the BigInsight Center for Research-driven Innovation, project number 237718, and Integreat Center of Excellence, project number 332645. LHBO wishes to thank Ingrid Kristine Glad and Kjersti Aas for their support.

Appendix

In Appendix A, we describe the implementation details. The link between the `paired average` and `paired kernel` strategies are discussed in Appendix B, while the corrected kernel weights are elaborated in Appendix C. Appendix D provides sina plots of the Shapley values computed in the main article. Additional sampling strategies are introduced and evaluated in Appendix E. In Appendix F, we compare the `paired cel-kernel` and `paired ceps-kernel` strategies. In Appendix G, we demonstrate that our novel techniques can significantly enhance the strategy used in the SHAP Python library.

A Implementation Details

We use version 0.2.3.9200 of the `shapr`-package in R available on GitHub (Sellereite and Jullum 2019) as a code foundation. In this version, the only sampling strategy in the package is the `unique` strategy from Section 3.1. We have implemented the other strategies introduced in Sections 3.2 to 3.7 and Appendix E. To generate the true contribution functions and Shapley values in Section 4.1, we have used the `gaussian` approach in `shapr` with $K = 5000$ Monte Carlo Samples from the true Gaussian data distribution. While we used explicit formulas for the contribution function in Section 4.2. In Section 5, we used the `random forest separate regression` approach introduced in Olsen et al. (2024) to compute the contribution functions. For the pilot estimates in Appendix E, we use the `linear model separate regression` approach introduced in Olsen et al. (2024) due to its rapid computations. We run the code on a shared computer server running Red Hat Enterprise Linux 8.5. The server has two Intel(R) Xeon(R) Gold 6226R CPU@2.90GHz (16 cores, 32 threads each) and 768GB DDR4 RAM. Since the memory usage is limited, all simulations can be run on a desktop computer, but at cost of increased elapsed time. Computing the exact Shapley values are the most computational demanding.

B From Paired Average to Paired Kernel

In Figure 13, we illustrate that the MAE curves corresponding to the `paired average` strategy converges (and worsens) to the MAE curves corresponding to the `paired kernel` strategy when we continue to sample coalitions. That is, we sample the chosen N_S unique coalitions an additional L times to make the corresponding sampling frequencies more accurate estimates of the Shapley kernel weights. We observe a gradual increase in the MAE when we increase L . This demonstrates that the stabilized sampling frequencies are better weights than the Shapley kernel weights when approximating Shapley values using the `KernelSHAP` framework.

C The Corrected Kernel Weights

In Table 3 and Figure 14, we extend Table 2 and Figure 2, respectively, to $M \leq 20$. We omit $M \leq 6$ due to the limited number of coalitions in these dimensions. Since, (14) equals one for all coalition sizes when $L = 2$, we have that the normalized weight curves over the non-trivial coalitions start at $(2^M - 2)^{-1}$. The curves related to the smaller and larger coalition sizes increase and decrease, respectively, from the starting value to the corresponding normalized Shapley kernel weights. The 95% confidence bands based on 1000 simulations of L are often quite narrow. We see that the dotted black lines, corresponding to the weights obtained by using $\mathbb{E}[L]$ given in (18) are located in the middle of the confidence bands. The dashed curves in Table 3 corresponds to the weights used by the `paired imp c-kernel` strategy and do not converge to the normalized Shapley kernel weights.

In Figures 15 and 16, we plot the values of the thousand simulated L values together with the empirical mean \bar{L} and the expectation $\mathbb{E}[L]$ given in (18). We see that the magnitude of L and the width of the confidence bands drastically increase when N_S approaches 2^M . This increase is natural as the probability of sampling the few remaining coalitions is tiny. The \bar{L} is 1233 for $M = 7$ when $N_S = 2^M - 2$ and \bar{L} increases on average by a factor of 2.35 each time M is increased by one.

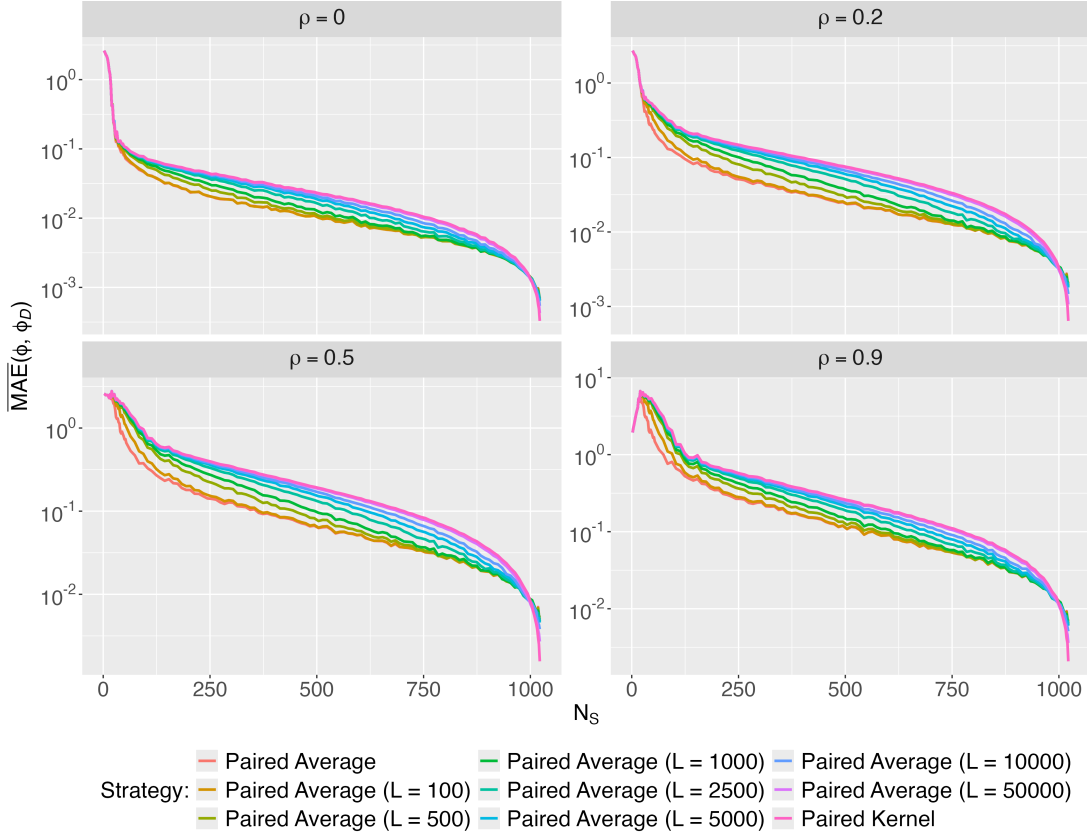


Figure 13: The $\overline{\text{MAE}}_{50}(\phi, \phi_D)$ values for the **paired average** strategy tend to the values obtained by the **paired kernel** strategy when sampling the $N_S = |\mathcal{D}|$ coalitions an additional L times.

D Sina Plots of the Shapley Values

In Sections 4 and 5, we discussed that the MAE scores have to be interpreted in connection to the magnitude of the Shapley values/function f , and we used averages to pinpoint what we considered a low MAE. In this section, we provide sina plots, also called beeswarm plots, to illustrate the different scales of the Shapley values; hence, using averages gives a rough estimate. In Figures 17 to 19, we include sina plots of the Shapley values ϕ in the simulation studies and examples in Sections 4.1, 4.2 and 5. For the simulation studies, we see that the magnitude of the Shapley values for X_1 , X_7 and X_{15} are larger than the other features, which makes sense due to their larger coefficients compared to the other features in the data generating processes. We also see that the Shapley values are more evenly distributed among the features for larger feature dependencies, a well-known property of the conditional Shapley value framework (Chen et al. 2020).

E Additional Sampling Strategies

We have investigated more sampling strategies than those discussed in Section 3, but we excluded them due to their very similar or generally poor performance. However, for the sake of completeness, we provide an overview of the strategies in Appendix E.1 and we elaborate on the two piloted strategies in Appendices E.2 and E.3. In Appendix E.4, we compare and evaluate the strategies on the same experiments as in Sections 4 and 5.

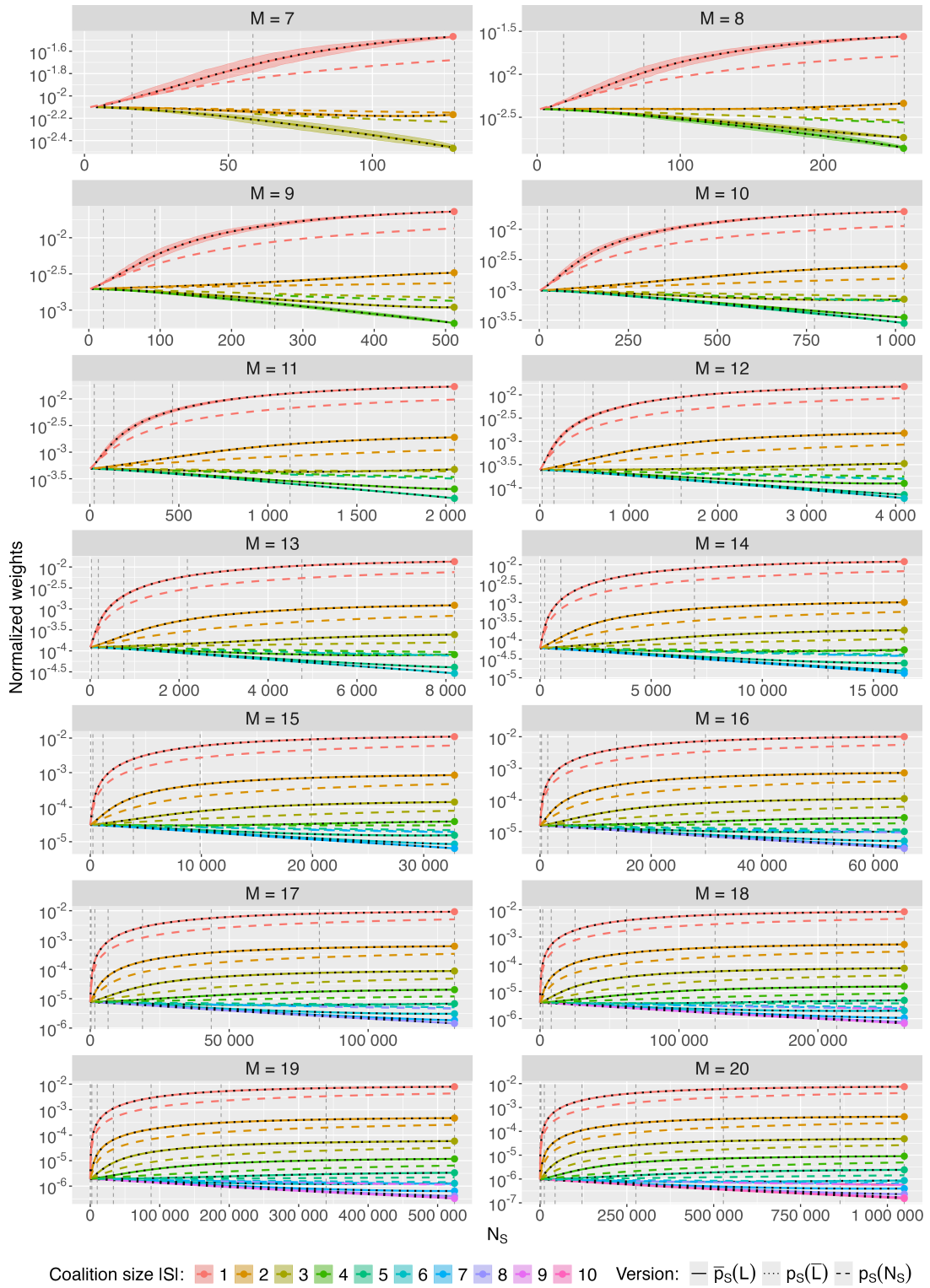


Figure 14: Extension of Figure 2 to $M \in \{7, 8, \dots, 20\}$. See Figure 2 for explanation of the curves and corresponding normalized Shapley kernel weights are provided in Table 3.

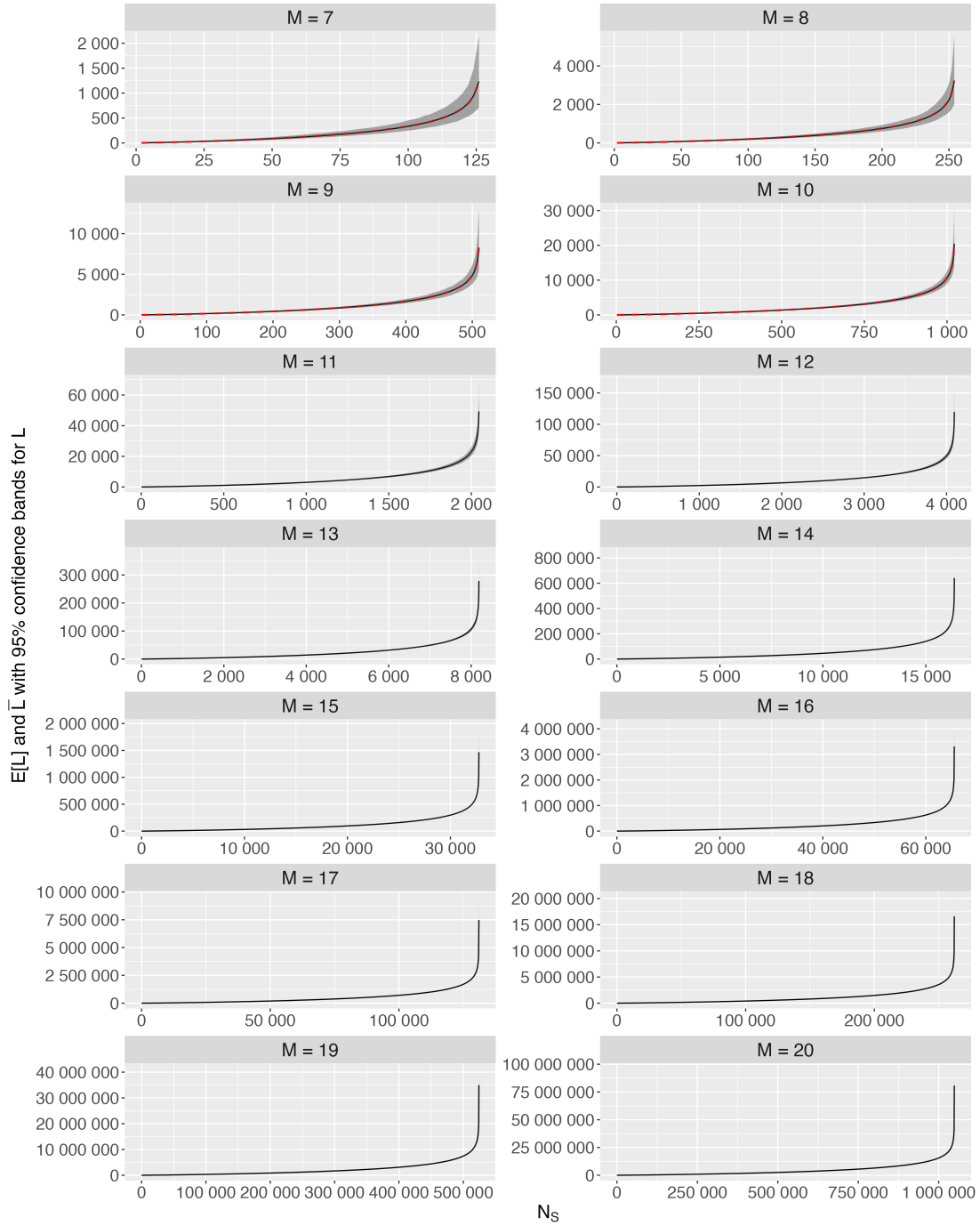


Figure 15: The mean \bar{L} and 95% confidence bands for the thousand simulated L values. The dashed red lines correspond to $\mathbb{E}[L]$ given in (18). The confidence bands get wider when N_S increases. For the larger M values, the confidence bands are narrow compared to the magnitude of L and are therefore difficult to see.

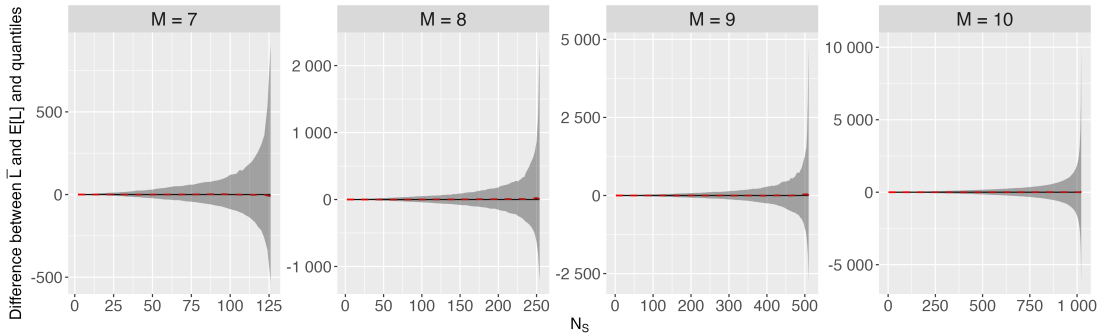


Figure 16: An extension of Figure 15, where we subtract \bar{L} to easier see the width of the confidence bands and the difference between \bar{L} and $\mathbb{E}[L]$.

M	$ \mathcal{S} = 1$	$ \mathcal{S} = 2$	$ \mathcal{S} = 3$	$ \mathcal{S} = 4$	$ \mathcal{S} = 5$	$ \mathcal{S} = 6$	$ \mathcal{S} = 7$	$ \mathcal{S} = 8$	$ \mathcal{S} = 9$	$ \mathcal{S} = 10$
7	3.40e-2	6.80e-3	3.40e-3	—	—	—	—	—	—	—
8	2.75e-2	4.59e-3	1.84e-3	1.38e-3	—	—	—	—	—	—
9	2.30e-2	3.29e-3	1.10e-3	6.57e-4	—	—	—	—	—	—
10	1.96e-2	2.45e-3	7.01e-4	3.51e-4	2.81e-4	—	—	—	—	—
11	1.71e-2	1.90e-3	4.74e-4	2.03e-4	1.35e-4	—	—	—	—	—
12	1.51e-2	1.51e-3	3.34e-4	1.25e-4	7.17e-5	5.97e-5	—	—	—	—
13	1.34e-2	1.22e-3	2.44e-4	8.14e-5	4.07e-5	2.91e-5	—	—	—	—
14	1.21e-2	1.01e-3	1.83e-4	5.50e-5	2.44e-5	1.53e-5	1.31e-5	—	—	—
15	1.10e-2	8.45e-4	1.41e-4	3.84e-5	1.54e-5	8.53e-6	6.40e-6	—	—	—
16	1.00e-2	7.18e-4	1.10e-4	2.76e-5	1.00e-5	5.02e-6	3.35e-6	2.93e-6	—	—
17	9.24e-3	6.16e-4	8.80e-5	2.03e-5	6.77e-6	3.08e-6	1.85e-6	1.44e-6	—	—
18	8.55e-3	5.34e-4	7.13e-5	1.53e-5	4.70e-6	1.96e-6	1.07e-6	7.47e-7	6.64e-7	—
19	7.95e-3	4.68e-4	5.84e-5	1.17e-5	3.34e-6	1.28e-6	6.42e-7	4.09e-7	3.27e-7	—
20	7.42e-3	4.12e-4	4.85e-5	9.09e-6	2.42e-6	8.66e-7	4.00e-7	2.33e-7	1.70e-7	1.53e-7

Table 3: The normalized Shapley kernel weights $p_{\mathcal{S}}$ in (8) for different values of M and coalition sizes.

E.1 Sampling Strategies: Overview

In this section, we provide an overview of the additional sampling strategies that we explored and we split them into two lists. In the first list, we introduce the additional strategies whose results we include in Appendix E.4, while the second list contains the strategies that are excluded due to their poor performance. The strategies ending with `kernel` and `empirical` use the Shapley kernel weights (Section 3.4) and the empirical mean sampling frequencies (explained below), respectively.

Paired empirical: The `paired empirical` strategy extends the `paired average` strategy by repeating the sampling step to obtain a more stable estimate of the weights for each coalition size, i.e., reduce their variance. That is, we repeat the sampling procedure 250 times and use the empirical means as the new weights. This extra sampling step is independent of the model and explicands and only depends on the number of features. Thus, these weights can be precomputed, stored, and used when applicable. This strategy performs very similar to the `paired c-kernel` and `paired cel-kernel` strategies.

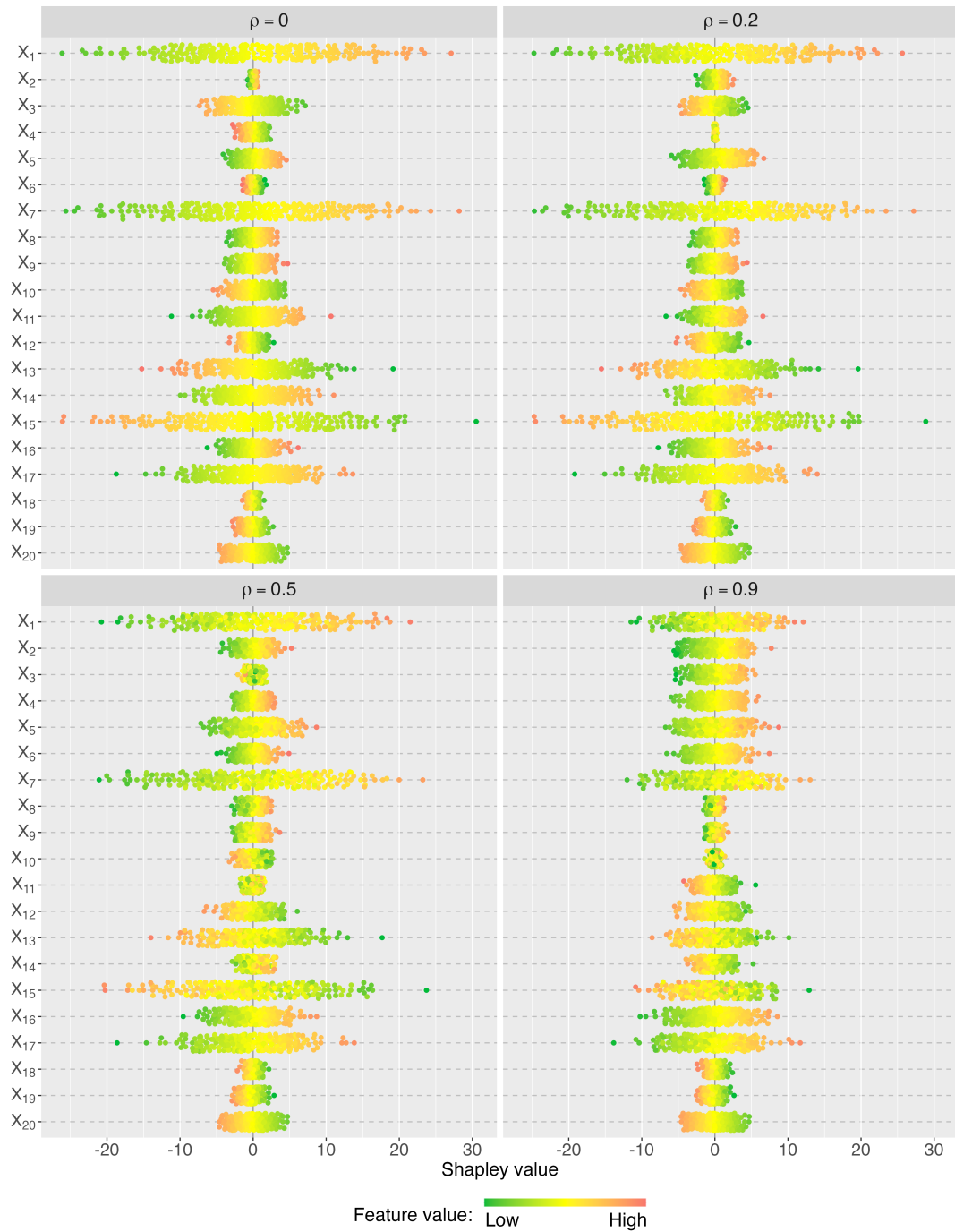


Figure 17: Sina plots of the exact Shapley values in the linear simulation study in Section 4.2.

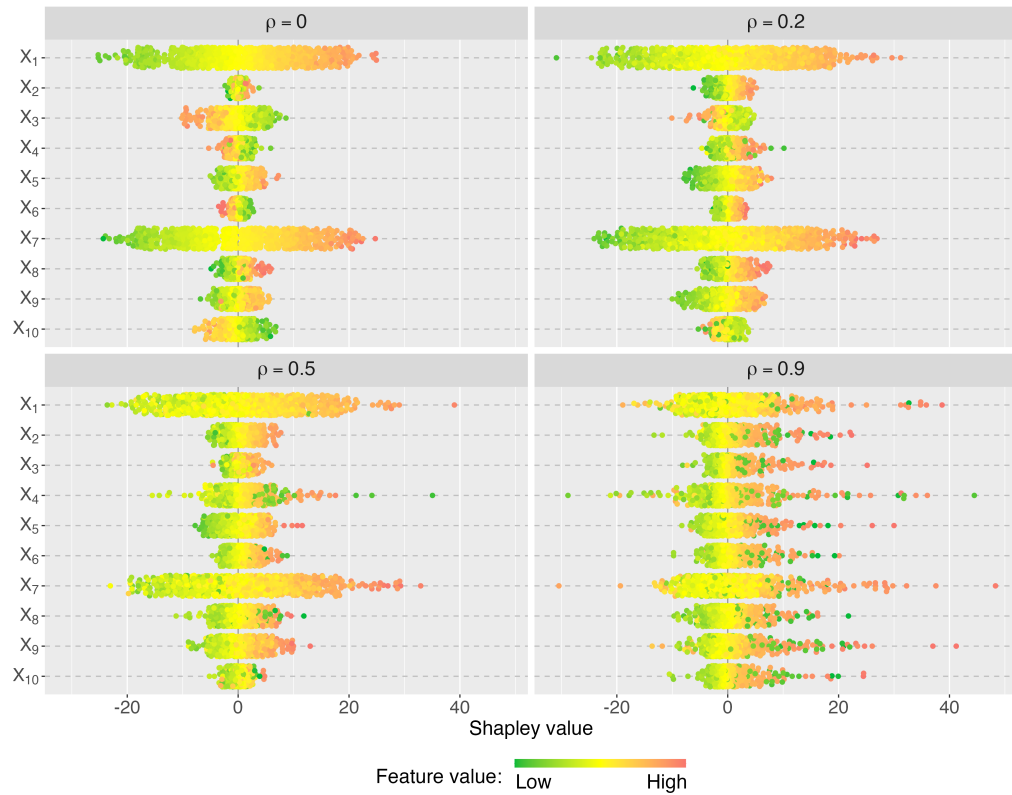


Figure 18: Sina plots of the exact Shapley values in the XGBoost simulation study in Section 4.1.

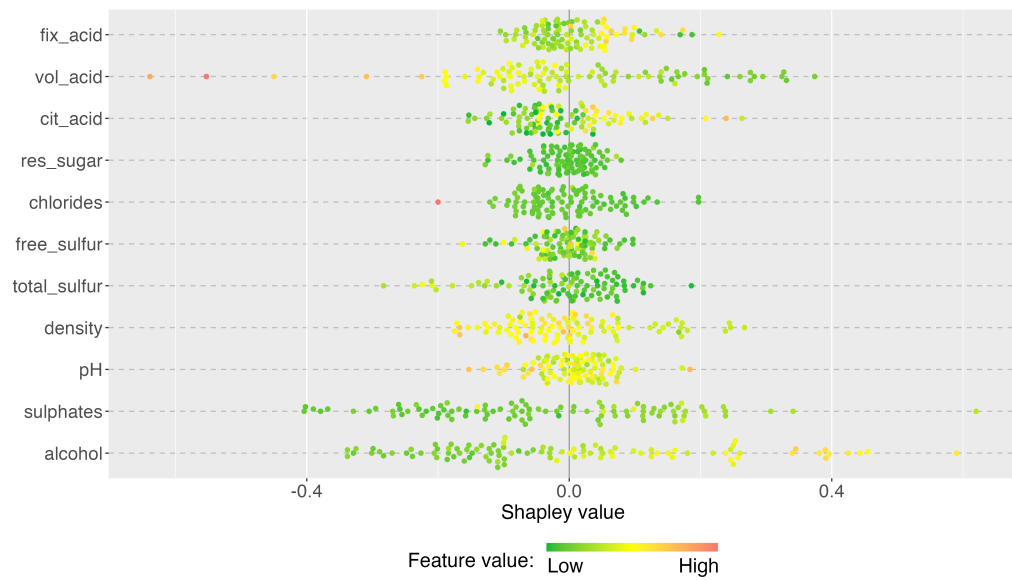


Figure 19: Sina plots of the exact Shapley values in the real-world data example in Section 5.

Paired largest empirical: The **paired largest empirical** strategy uses the empirical mean weights introduced by the **paired empirical** strategy but rather includes paired coalitions based on their weights in decreasing order, as the **paired imp c-kernel** strategy in Section 3.7. This strategy performs very similar to the **paired imp cel-kernel** strategy.

Paired largest kernel: This strategy is equivalent to the **paired largest empirical** strategy except for using the Shapley kernel weights instead of the empirical mean sampling frequencies. That is, we add the coalitions with the largest Shapley kernel weights first in increasing order and paired manner. Then we sample coalitions with uniform probability for the coalition size where not all coalitions are included.

Paired largest order kernel: Identical to the **paired largest kernel** strategy except that we rather add the coalitions in order and paired manner for coalition sizes where not all coalitions are included. To elaborate, in the example given in Section 3.7, the latter three coalitions would be $\{1, 2, 3\}$, the pair $\{4, 5, 6, 7, 8, 9, 10\}$, and $\{1, 2, 4\}$. Then we use the Shapley kernel weights.

Paired largest order empirical: Identical to the **paired largest order kernel** strategy except that we use the empirical mean sampling frequencies as the weights.

Pilot average: Identical to the **paired average** strategy except that we sample the coalitions using the piloted importance weights for each coalition introduced in Appendix E.2 instead of using the Shapley kernel weights. This means that the distribution of the stabilized sampling frequencies will not tend to the Shapley kernel weights, and the strategy will give inaccurate approximations when $N_S \rightarrow 2^M$.

Pilot empirical: Identical to the **pilot average** strategy except that we replace the sampling frequencies at the end with the empirical mean sampling frequencies. Conceptually, this ensures that we sample important coalitions but weigh them such that we obtain the exact Shapley values when $N_S \rightarrow 2^M$.

Pilot largest kernel: We add the coalitions based on the order of importance based on the pilot estimates and then use the Shapley kernel weights. That is, no sampling is conducted.

Pilot largest empirical: Identical to the **pilot largest kernel** strategy except that we use the empirical mean sampling frequencies as the weights.

MAD largest kernel: Identical to the **paired largest kernel** strategy except that instead of sampling the remaining coalitions, we use the procedure outlined in Appendix E.3 to determine the most important coalitions and include them based on the order of importance. Then we use the Shapley kernel weights.

MAD largest empirical: Identical to the **MAD largest kernel** strategy except that we use the empirical mean sampling frequencies as the weights.

We now present the strategies not included in Appendix E.4 as they performed poorly.

Order increasing kernel: Add coalitions based on the ordering introduced in the Section 3. That is, we add all coalitions of size one, then size two, and so on.

Order decreasing kernel: Add coalitions based on the reverse ordering introduced in the Section 3. That is, we add all coalitions of size $M - 1$, then size M_2 , and so on.

Paired smallest kernel: Add coalitions with the smallest Shapley kernel weights first in decreasing order and paired manner. I.e., the reverse order of the **paired largest kernel** strategy.

Largest coalition kernel: Add the coalitions with the largest Shapley kernel weights first but in increasing coalition size (i.e., no paired sampling). E.g., for $M = 4$, we would add the coalitions in the following order: $\{1\}$, $\{2\}$, $\{3\}$, $\{4\}$, $\{1, 2, 3\}$, $\{1, 2, 4\}$, $\{1, 3, 4\}$, $\{2, 3, 4\}$, $\{1, 2\}$, $\{1, 3\}$, $\{1, 4\}$, $\{2, 3\}$, $\{2, 4\}$, and $\{3, 4\}$.

Smallest coalition kernel: Add the coalitions with the smallest Shapley kernel weights first but in decreasing coalition size (i.e., no paired sampling). I.e., the reverse order of the **largest coalition kernel** strategy.

E.2 Sampling Strategies: Pilot

The pilot strategies are motivated by the fact that some coalitions often are more critical than others in the Shapley value computations. Thus, we should include these coalitions when approximating the Shapley values. The strategies in Section 3 sample the coalitions only based on the coalition size $|\mathcal{S}|$ and do not take $v(\mathcal{S})$ into consideration (as they are not available). We propose to compute (rough) pilot estimates $\tilde{v}(\mathcal{S})$ of $v(\mathcal{S})$ and include these in the sampling procedure. We use a linear regression model to estimate $v(\mathcal{S})$, i.e., the **linear model separate regression** approach in Olsen et al. (2024). This approach was chosen for its low computational cost.

It is conceptually possible that all coalitions are important for some combinations of features and explicands. However, this is not optimal as we want to limit the number of coalitions \mathcal{S} to compute $v(\mathcal{S})$ for. Thus, we average across the features and explicands to determine the $N_{\mathcal{S}}$ most important coalitions on average and use those for all features and explicands. Let \mathbf{R}^* be the \mathbf{R} matrix in (6) but where we have removed the first row. The first row is 1 in the first column and 0 in the remaining columns and is used to compute $\phi_0 = v(\emptyset)$. Thus,

$$\mathbf{R}^* = \begin{bmatrix} R_{1,1} & R_{1,2} & \dots & R_{1,2^M-1} & R_{1,2^M} \\ R_{2,1} & R_{2,2} & \dots & R_{2,2^M-1} & R_{2,2^M} \\ \vdots & \vdots & \ddots & \vdots & \vdots \\ R_{M-1,1} & R_{M-1,2} & \dots & R_{M-1,2^M-1} & R_{M-1,2^M} \\ R_{M,1} & R_{M,2} & \dots & R_{M,2^M-1} & R_{M,2^M} \end{bmatrix}$$

and the remaining Shapley values for a particular explicand is then $\mathbf{R}^* \mathbf{v}$. By using the order of coalitions that we specified in Section 3, we can write the j th Shapley value as $\phi_j = \sum_{k=1}^{2^M} R_{j,k} v(\mathcal{S}_k)$, for $j = 1, 2, \dots, M$. Here $\mathcal{S}_1 = \emptyset$ and $\mathcal{S}_{2^M} = \mathcal{M}$.

To investigate the importance of each coalition in the Shapley value, we can compute the element-wise product between \mathbf{R}^* and \mathbf{v} and look at the magnitude of the elements. That is,

$$\mathbf{R}^* \otimes \mathbf{v} = \begin{bmatrix} R_{1,1}v(\mathcal{S}_1) & R_{1,2}v(\mathcal{S}_2) & \dots & R_{1,2^M-1}v(\mathcal{S}_{2^M-1}) & R_{1,2^M}v(\mathcal{S}_{2^M}) \\ R_{2,1}v(\mathcal{S}_1) & R_{2,2}v(\mathcal{S}_2) & \dots & R_{2,2^M-1}v(\mathcal{S}_{2^M-1}) & R_{2,2^M}v(\mathcal{S}_{2^M}) \\ \vdots & \vdots & \ddots & \vdots & \vdots \\ R_{M-1,1}v(\mathcal{S}_1) & R_{M-1,2}v(\mathcal{S}_2) & \dots & R_{M-1,2^M-1}v(\mathcal{S}_{2^M-1}) & R_{M-1,2^M}v(\mathcal{S}_{2^M}) \\ R_{M,1}v(\mathcal{S}_1) & R_{M,2}v(\mathcal{S}_2) & \dots & R_{M,2^M-1}v(\mathcal{S}_{2^M-1}) & R_{M,2^M}v(\mathcal{S}_{2^M}) \end{bmatrix}.$$

We explored treating each column/coalition separately, but we obtained better results when we paired each coalition with its complement. Thus, we subtract the $2^M + 1 - i$ th column from the i th column for $i = 1, 2, \dots, 2^M - 1$. Since $R_{j,i} = -R_{j,2^M+1-i}$, for $i = 1, 2, \dots, 2^M$, we can write the differences as

$$\mathbf{T} = \begin{bmatrix} R_{1,1}(v(\mathcal{S}_1) + v(\mathcal{S}_{2^M})) & R_{1,2}(v(\mathcal{S}_2) - v(\mathcal{S}_{2^M-1})) & \dots & R_{1,2^M-1}(v(\mathcal{S}_{2^M-1}) + v(\mathcal{S}_{2^M-1+1})) \\ R_{2,1}(v(\mathcal{S}_1) + v(\mathcal{S}_{2^M})) & R_{2,2}(v(\mathcal{S}_2) - v(\mathcal{S}_{2^M-1})) & \dots & R_{2,2^M-1}(v(\mathcal{S}_{2^M-1}) + v(\mathcal{S}_{2^M-1+1})) \\ \vdots & \vdots & \ddots & \vdots \\ R_{M-1,1}(v(\mathcal{S}_1) + v(\mathcal{S}_{2^M})) & R_{M-1,2}(v(\mathcal{S}_2) - v(\mathcal{S}_{2^M-1})) & \dots & R_{M-1,2^M-1}(v(\mathcal{S}_{2^M-1}) + v(\mathcal{S}_{2^M-1+1})) \\ R_{M,1}(v(\mathcal{S}_1) + v(\mathcal{S}_{2^M})) & R_{M,2}(v(\mathcal{S}_2) - v(\mathcal{S}_{2^M-1})) & \dots & R_{M,2^M-1}(v(\mathcal{S}_{2^M-1}) + v(\mathcal{S}_{2^M-1+1})) \end{bmatrix}.$$

Recall that the \mathbf{T} matrix is explicand specific, hence, let $\mathbf{T}^{[i]}$ denote the matrix for the i th explicand. We can then look at the $|\mathbf{T}_{j,k}^{[i]}|$ quantities and average them over the features j and explicands i to see which coalitions k that have the largest absolute effect on the Shapley values.

To better understand the pilot idea, consider a small 5-dimensional toy-example where we have computed the exact $v(\mathcal{S})$ quantities for a linear model with coefficients $\boldsymbol{\beta} = [2, 10, 0.25, -3, -1, 1.5]$ and the data is generated according to a multivariate Gaussian distribution with mean zero and an equi-correlation matrix with $\rho = 0.5$. In Figure 20, we illustrate the corresponding $|\mathbf{T}_{j,k}^{[i]}|$ quantities

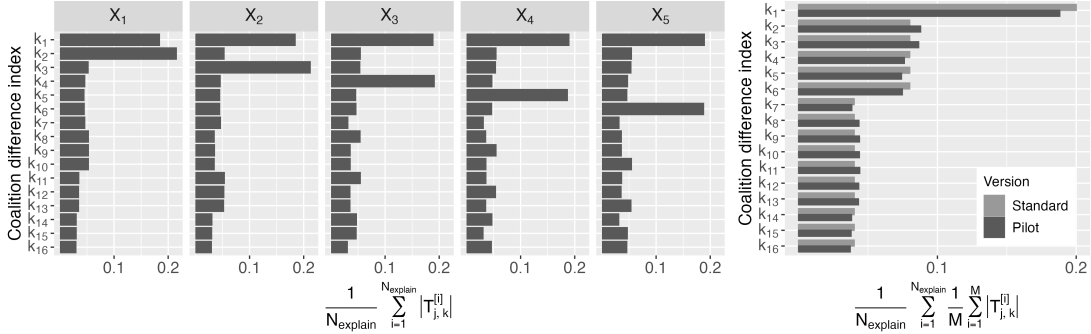


Figure 20: The (normalized) $|\mathbf{T}_{j,k}^{[i]}|$ pilot weights when averaged over the explicands (left) and also over the features (right). Standard corresponds to all coalitions of the same size having equal importance.

when averaged only over the explicands and when averaged over both the explicands and features. When only averaged over the explicands, we see that the most important coalition pair for the j th feature is when j is the only feature in \mathcal{S} . When we also average over the features, we obtain slightly different weights than when giving all coalitions of the same size the same importance. Ideally, these differences should reflect the importance of the coalition.

We can then add the coalitions in the order of largest importance and use the Shapley kernel weights or the empirical means as the weights. We name these strategies for **pilot largest kernel** and **pilot largest empirical**, respectively. Another strategy is to sample the coalitions using these modified weights. However, the approximations will then not converge to the true Shapley values when $N_{\mathcal{S}}$ increases as we do not sample from the Shapley kernel distribution. We then use over stabilizing technique as in **paired average** and call the corresponding strategy for **pilot average**. In the **pilot empirical** strategy, we replace the final weights with the empirical mean weights.

In further work, we would like to investigate methods for obtaining better and faster pilot estimates (in settings where a linear model is too expensive). Especially in higher dimensions, as we would then most likely have to sample a subset of features, compute pilot estimates of them, and then sample a new subset from the sampled coalitions.

E.3 Sampling Strategies: MAD

Here we modify the **paired largest empirical** strategy to not add the coalitions randomly, but by using pilot estimates to determine the most important coalitions and then add them. The following setup differs from Appendix E.2 in that we do not need pilot estimates for the relevant coalition size, i.e., where **paired largest empirical** sampled coalitions. This means that the number of pilot estimates is reduced from 2^M to $\binom{M}{|\mathcal{S}|}$ when $|\mathcal{S}| = |\bar{\mathcal{S}}|$ and $2\binom{M}{|\mathcal{S}|}$ when $|\mathcal{S}| \neq |\bar{\mathcal{S}}|$.

For an important subset of features, we should have that $v(\mathcal{S})$ is close to $f(\mathbf{x})$, as this tells us that the features in \mathcal{S} can model f accurately. We therefore rank the coalitions based on the *mean absolute difference* $\text{MAD}(\mathcal{S}) = \frac{1}{N_{\text{explain}}} \sum_{i=1}^{N_{\text{explain}}} |v(\mathcal{S}; \mathbf{x}_i) - f(\mathbf{x}_i)|$. Coalitions containing less than half the features contain important features if the MAD is low. While the MAD is high for coalitions containing more than half the features but where important features are missing. For coalitions where $|\mathcal{S}| = |\bar{\mathcal{S}}| = M/2$ (only for M even), then we order the coalitions based on increasing MAD. For coalitions where $|\mathcal{S}| \neq |\bar{\mathcal{S}}|$, we order the coalitions in an increasing paired manner based on the difference between $\text{MAD}(\mathcal{S})$ and $\text{MAD}(\bar{\mathcal{S}})$. A potential modification to the **MAD largest** strategy to make it stochastic is to use the scaled inverse mean absolute distance $\text{MAD}^{-1}(\mathcal{S})$ as weights.

E.4 Sampling Strategies: Results

The results of the additional strategies for the XGBoost and linear experiments are provided in Figures 21 and 22, respectively. For the linear experiment, we have reduced M from twenty to seventeen and use the first seventeen coefficients and rows/columns in the block equi-correlation matrix. While the results for the Red Wine data set experiment is provided in Figure 23. Additionally, we use fewer repetitions B and a coarser set of N_S values. To more easily compare Figures 21 and 22 with Figures 3, 7 and 10 we include the **paired kernel** strategy in all figures, while the **paired empirical** and **paired largest empirical** strategies can be thought of as proxies for the **paired cel-kernel** and **paired imp cel-kernel** strategies as their performance is more or less identical. Thus, we only include the former two. For all experiments, we see that the additional strategies perform on par or worse than the strategies included in Section 4. The **kernel** based strategies perform worse than the empirical strategies. The performance of the strategies in the Red Wine data set is closer to those observed in the linear than in the XGBoost experiments.

By comparing the **paired largest empirical** and **paired largest order empirical** strategies, we see that randomly adding the coalitions is better than adding them based on the chronological coalition order introduced in Section 4. This is intuitive, as the random order over B repetitions will better explore the importance of the coalitions than the single deterministic order. However, they match up at the dashed vertical lines when all coalitions of a given size are included.

The motivation behind the **MAD largest empirical** and **pilot largest empirical** is to determine the best order to add the coalitions based on pilot estimates. However, neither strategy outperforms the random inclusion done in the **paired largest empirical** strategy. We observe (more or less) identical curves when we use the true $v(\mathcal{S})$ quantities as the pilot estimates $\tilde{v}(\mathcal{S})$ (figures not included). This implies that imprecise pilot estimates are not to blame but rather that the setups in Appendices E.2 and E.3 are sub-optimal. Note that the strategies match up at the dashed vertical lines as they include all (paired) coalitions of one size before including coalitions of another size (see the weights in Figure 20). In a smaller-dimensional setup, brute force can be considered to try to discover the optimal coalitions to include, and then use this information to build intuition and create a better importance criterion than those proposed in Appendices E.2 and E.3.

The MSE curves related to the **pilot average** strategy are “U”-shaped. The rising errors when N_S increases are caused by sampling from a distribution different than the Shapley kernel distribution, meaning that our approximated Shapley values $\phi_{\mathcal{D}}$ will not converge to ϕ when N_S increases.

All the kernel-based strategies (**paired kernel**, **paired largest kernel**, **paired largest order kernel**, **pilot largest kernel**, and **MAD largest kernel**) perform similarly to each other, and worse than the empirical-based counter strategies. Furthermore, the **paired kernel** is often the worst, which means that randomly selecting the coalitions is worse than adding the coalitions based on, e.g., the decreasing order of the magnitude of the Shapley kernel weights.

The erratic behavior of the **MAD largest kernel** and **MAD largest empirical** strategies in Figure 21 for $|\mathcal{S}| = 5$ is due to the procedure described in Appendix E.3 not doing paired sampling when $|\mathcal{S}| = \bar{S}$. This only happens when M is even, hence we do not see the same behavior in Figures 21 and 23. This illustrates the importance of paired sampling and how it stabilizes and improves the approximations. A potential modification/fix would be to also enforce pairing in the $|\mathcal{S}| = |\bar{S}|$ setting.

F Comparing Paired CEL-Kernel and Paired CEPS-Kernel

In this section, we illustrate that using (19) with $\mathbb{E}[L]$ or employing $w_S \propto \mathbb{E}[\tilde{p}_S]$ yields equally precise Shapley value approximations in our simulation studies. To estimate $\mathbb{E}[\tilde{p}_S]$, we simulate 1000 L values, compute \tilde{p}_S for each, and then take the mean. We refer to this method as the **paired ceps-kernel** strategy. In Figures 24 and 25, we plot the relative difference between the **paired cel-kernel** and **paired ceps-kernel** strategies, with the former as the reference, for the simulation study in Sections 4.1 and 4.2, respectively. We clearly see that their performance is more or less equivalent. The figures for the real-world experiment in Section 5 (not included) tell the exact same story, indicating that there is no meaningful difference between the two strategies in our simulation studies and experiments.

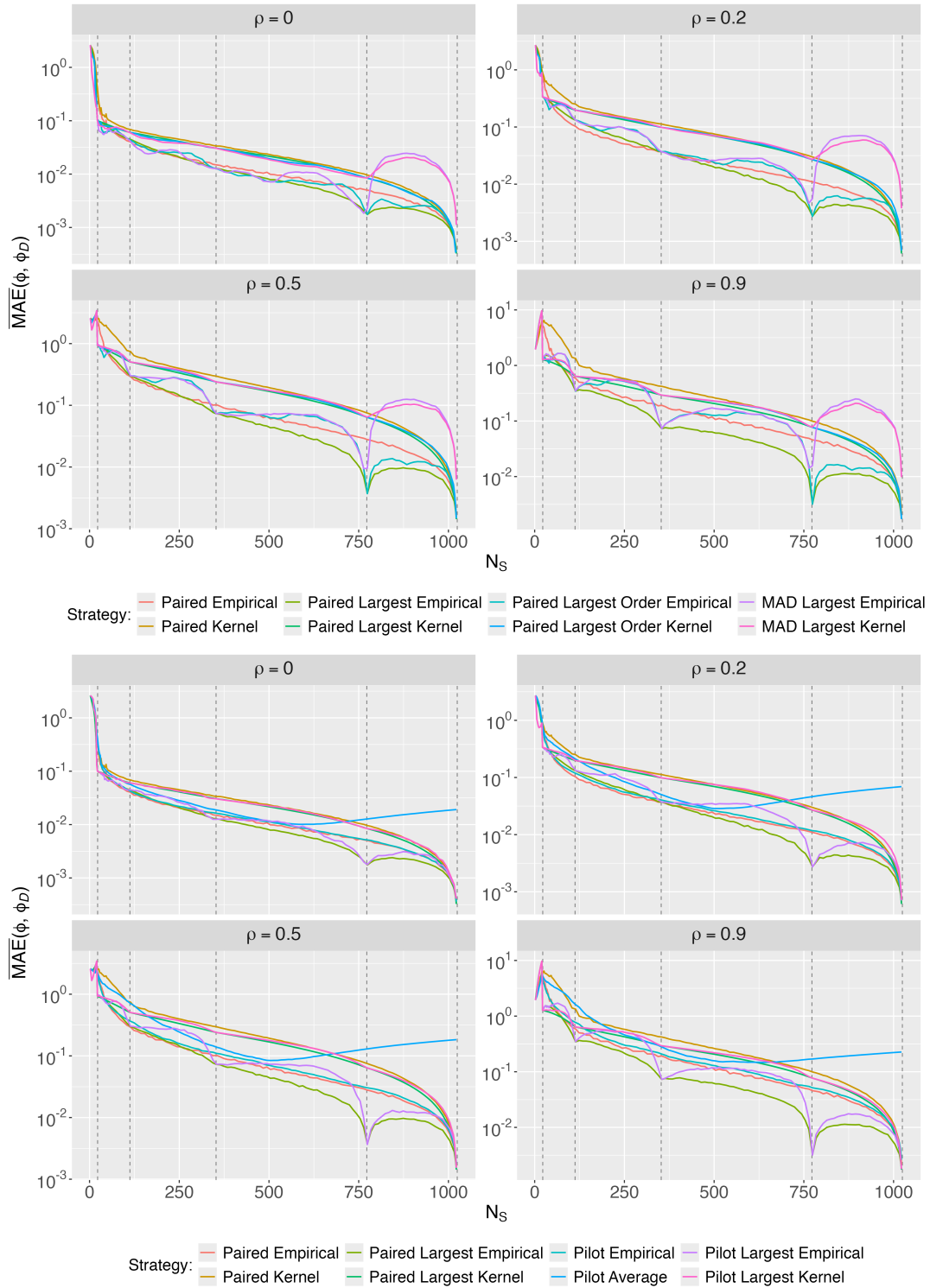


Figure 21: XGBoost experiment (Section 4.1): $\overline{\text{MAE}}_{50}(\phi, \phi_D)$ for different number of coalitions N_S and dependencies levels ρ on log-scale.

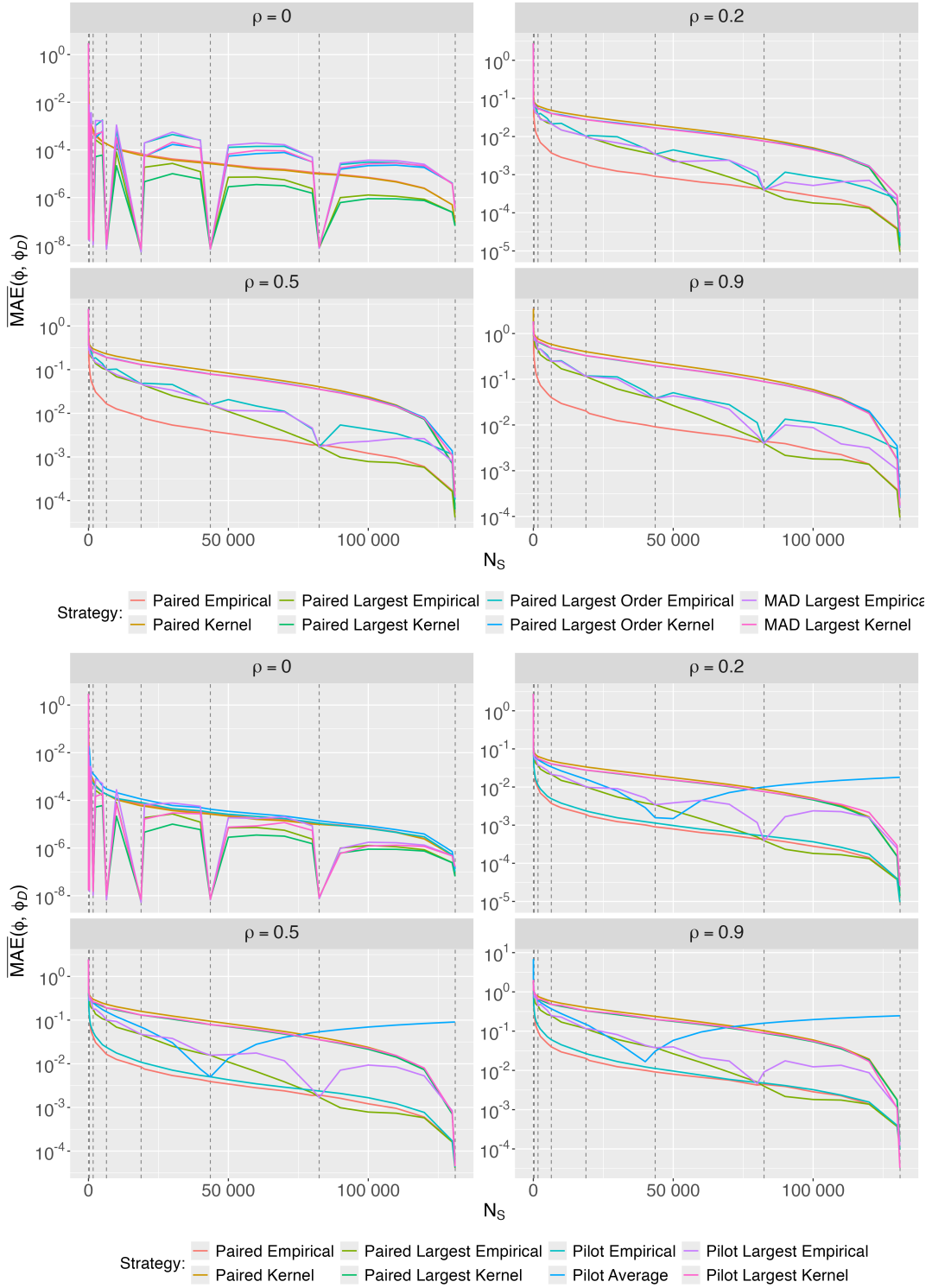


Figure 22: Linear experiment (Section 4.2): $\overline{\text{MAE}}_{10}(\phi, \phi_D)$ for different number of coalitions N_S and dependencies levels ρ on log-scale.

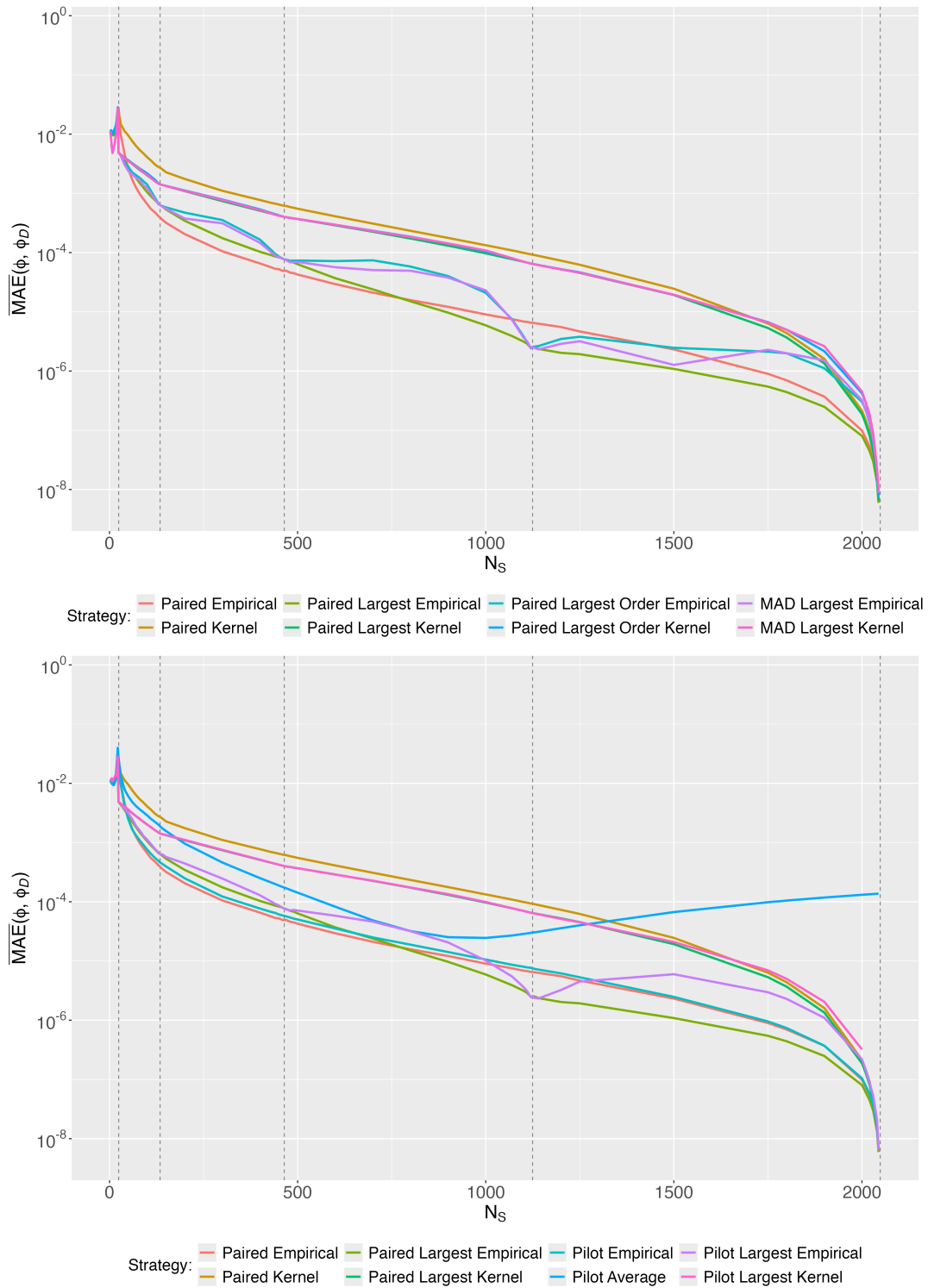


Figure 23: Red Wine data set experiment (Section 5): $\overline{\text{MAE}}_{25}(\phi, \phi_D)$ for different number of coalitions N_S and dependencies levels ρ on log-scale.

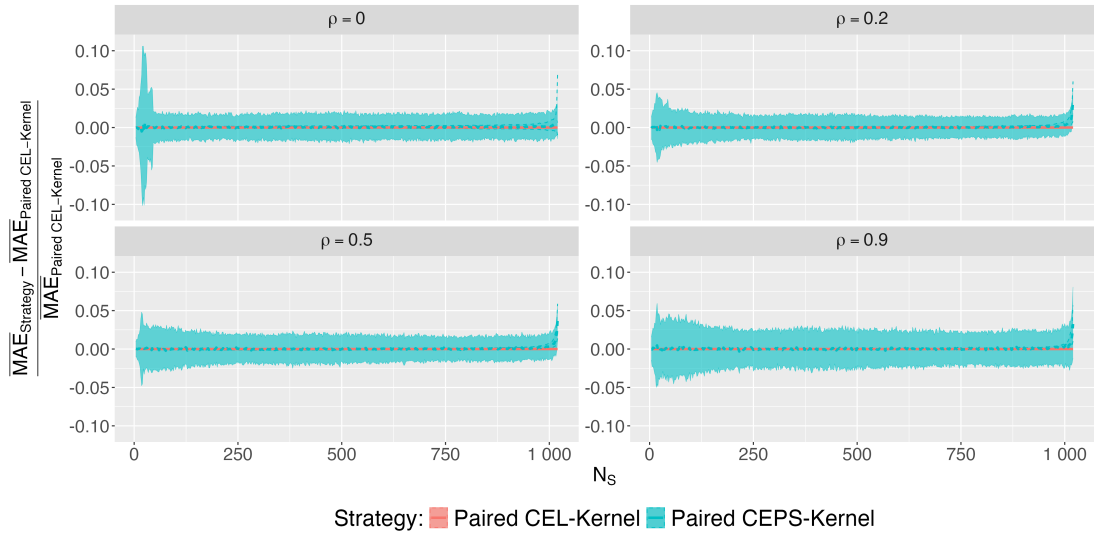


Figure 24: XGBoost experiment: the relative $\overline{\text{MAE}}_{500}(\phi, \phi_{\mathcal{D}})$ difference between the **paired cel-kernel** and **paired ceps-kernel** strategies, with the former as the reference. The solid and dashed confidence bands are 95% confidence bands for the relative $\overline{\text{MAE}}_{500}$ and MAE_b differences, respectively. Lower values are better.

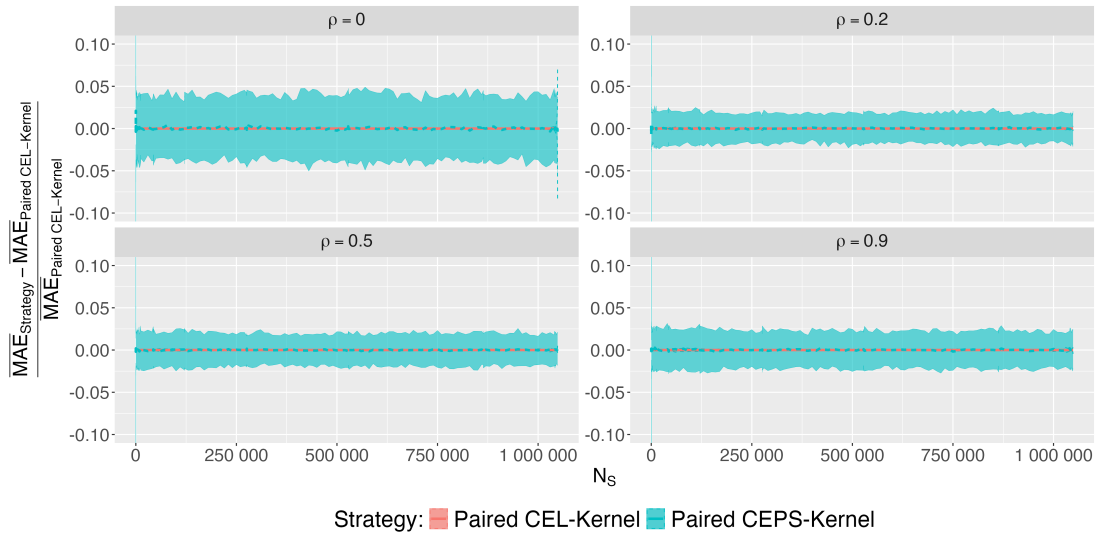


Figure 25: Linear experiment: the relative $\overline{\text{MAE}}_{150}(\phi, \phi_{\mathcal{D}})$ difference between the **paired cel-kernel** and **paired ceps-kernel** strategies, with the former as the reference. The solid and dashed confidence bands are 95% confidence bands for the relative $\overline{\text{MAE}}_{150}$ and MAE_b differences, respectively. Lower values are better.

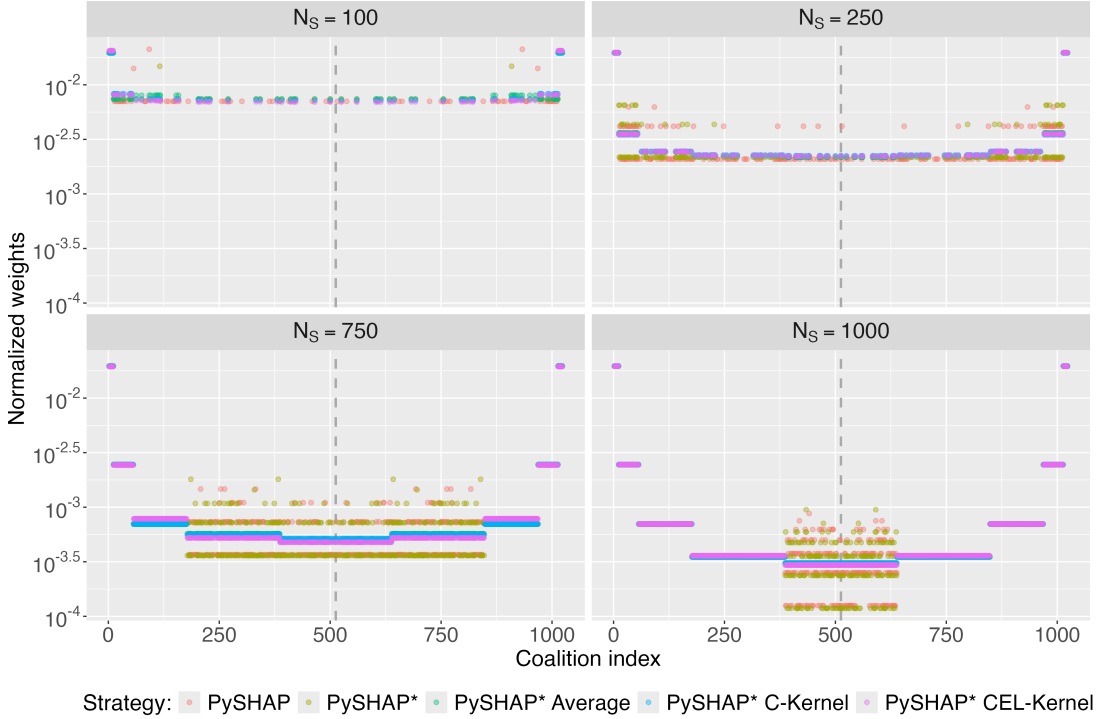


Figure 26: The normalized weights w_S used in (7) by the strategies introduced in Appendix G for different number of unique coalitions N_S in an $M = 10$ -dimensional setting. All strategies are symmetric around the vertical line, except the PySHAP strategy, which is non-symmetric in the middle-most coalition size of five as there $|\mathcal{S}| = |\bar{\mathcal{S}}|$.

G The SHAP Python Library

In this section, we demonstrate that our novel techniques can significantly enhance the strategy used in the popular SHAP Python library (Lundberg and Lee 2024), which we name PySHAP. We briefly explain PySHAP below, while more detailed descriptions can be found in Herren and Hahn (2022, Section 2.2.5) and Fumagalli et al. (2024, Appendix B). Upon examining the implementation of PySHAP in version 0.46.0 of SHAP (the latest version at the current date), we observed that it explicitly does *not* pair coalitions for the coalition size where $|\mathcal{S}| = |\bar{\mathcal{S}}|$, a condition only relevant if M is even. It remains unclear to us whether this is an intentional design choice or an oversight. Based on this finding, and drawing on the techniques discussed in Sections 3.3 and 3.5, we propose modifications to PySHAP at the end of this section and conduct benchmarking to assess their efficacy.

We now describe the sampling and weighting procedure in PySHAP before providing an illustrative example for clarity. The PySHAP strategy divides the sampling procedure into a deterministic and sampling-based part based on the number of unique coalitions N_S . It deterministically includes all coalitions of size $|\mathcal{S}|$ and $M - |\mathcal{S}|$ if the number of remaining coalitions to sample N_S^* exceeds the expected number of coalitions needed to sample all coalitions of these sizes, i.e., $2^{\binom{M}{|\mathcal{S}|}}$. The strategy begins with coalition size one and increments by one until the number of remaining coalitions N_S^* becomes insufficient. Denote the coalition size at which the PySHAP strategy stops by $P \in \{1, 2, \dots, \lceil (M+1)/2 \rceil\}$, where $\lceil \cdot \rceil$ is the ceiling function. All coalitions of size $|\mathcal{S}| < P$ and $|\mathcal{S}| > M - P$ are then included, and their corresponding weights are assigned according to the normalized Shapley kernel weight in (8). Figure 26 illustrates the deterministic inclusion of coalitions as a function of N_S , showing that more coalition sizes are included as N_S increases.

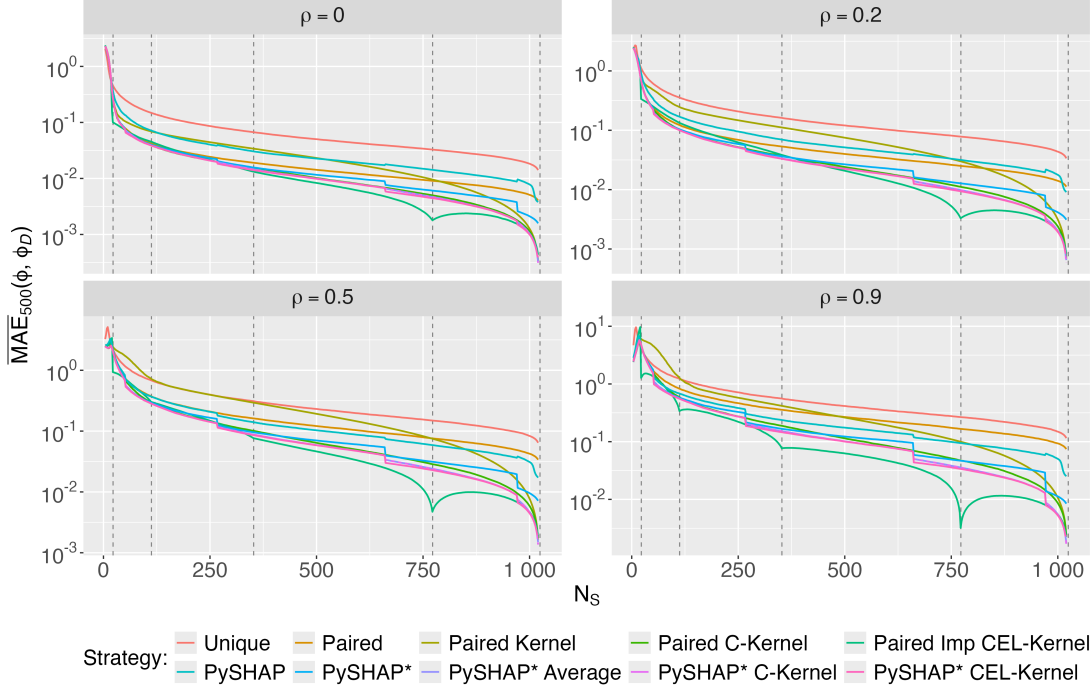


Figure 27: XGBoost experiment: $\text{MAE} = \overline{\text{MAE}}_{500}(\phi, \phi_{\mathcal{D}})$ for different number of coalitions $N_{\mathcal{S}}$ and dependencies levels ρ on log-scale using the strategies introduced in Appendix G. The **PySHAP* average** and **PySHAP* c-kernel** strategies are almost completely overlapping.

The remaining $N_{\mathcal{S}}^*$ coalitions are sampled with replacements from the non-included coalition sizes, i.e., $|\mathcal{S}| \in \llbracket P, M - P \rrbracket$, following a two-step procedure similar to the one described in Section 3.1. Here, $\llbracket a, b \rrbracket$ is the interval of all integers between a and b included. First, a coalition size $|\mathcal{S}| \in \llbracket P, M - P \rrbracket$ is selected with probability proportional to $p_{\mathcal{S}} \binom{M}{|\mathcal{S}|}$, where $p_{\mathcal{S}}$ is the normalized Shapley kernel weight for a coalition \mathcal{S} of size $|\mathcal{S}|$ as given in (8). Second, a coalition \mathcal{S} of size $|\mathcal{S}|$ is sampled among the $\binom{M}{|\mathcal{S}|}$ possible coalitions with uniform probability. The paired coalition $\bar{\mathcal{S}}$ is also included, except when $|\mathcal{S}| = |\bar{\mathcal{S}}|$, a situation that occurs only when M is even. The sampling frequencies are used as weights but scaled to sum to the remaining normalized Shapley kernel weights, i.e., $1 - 2 \sum_{q=1}^{P-1} p_q \binom{M}{q}$.

For the sake of clarity, consider an example with $M = 10$ and $N_{\mathcal{S}} = 100$, as illustrated in Figure 26. From Table 3, we have that the normalized Shapley kernel weight for a coalition of size one is $p_1 = 0.0196$. This means **PySHAP** includes the $2 \binom{10}{1} = 20$ coalitions of size one and nine when $N_{\mathcal{S}} \geq \frac{1}{0.0196} = 51.02$, which is the case in our example. The remaining number of coalitions is then $N_{\mathcal{S}}^* = 80$. The next step is to re-normalize the remaining Shapley kernel weights as given in Table 3, resulting in $\tilde{p}_2 = 0.00404$, $\tilde{p}_3 = 0.00116$, $\tilde{p}_4 = 0.00058$, and $\tilde{p}_5 = 0.00046$, such that $\sum_{q=2}^{\lfloor M/2 \rfloor} \tilde{p}_q \binom{M}{q} = 1$. Thus, **PySHAP** includes all coalitions of size two and eight if $N_{\mathcal{S}}^* > 1/0.00404 = 247.5$, which it is not. This implies that $N_{\mathcal{S}}$ must be greater or equal to 268 to include coalition sizes two and eight. Consequently, the remaining $N_{\mathcal{S}}^* = 80$ coalitions will be sampled by first selecting the coalition size $|\mathcal{S}|$ with probability $\tilde{p}_{\mathcal{S}} \binom{M}{|\mathcal{S}|}$, followed by uniformly sampling a coalition \mathcal{S} among the $\binom{M}{|\mathcal{S}|}$ coalitions of size $|\mathcal{S}|$. This procedure is repeated until $N_{\mathcal{S}}^*$ unique coalitions are sampled⁸, and the corresponding sampling frequencies are used as weights. However, the weights are scaled such that they sum to $1 - 2 \binom{M}{1} p_1 = 2 \times 10 \times 0.0196 = 0.608$.

⁸Originally, **PySHAP** stops sampling after reaching an upper limit of $4N_{\mathcal{S}}^*$ sampled coalitions, including duplicates, which means that the total number of unique coalitions can be less than $N_{\mathcal{S}}$. However, we disable this upper limit to ensure a fair comparison with the other strategies, which utilize $N_{\mathcal{S}}$ unique coalitions.

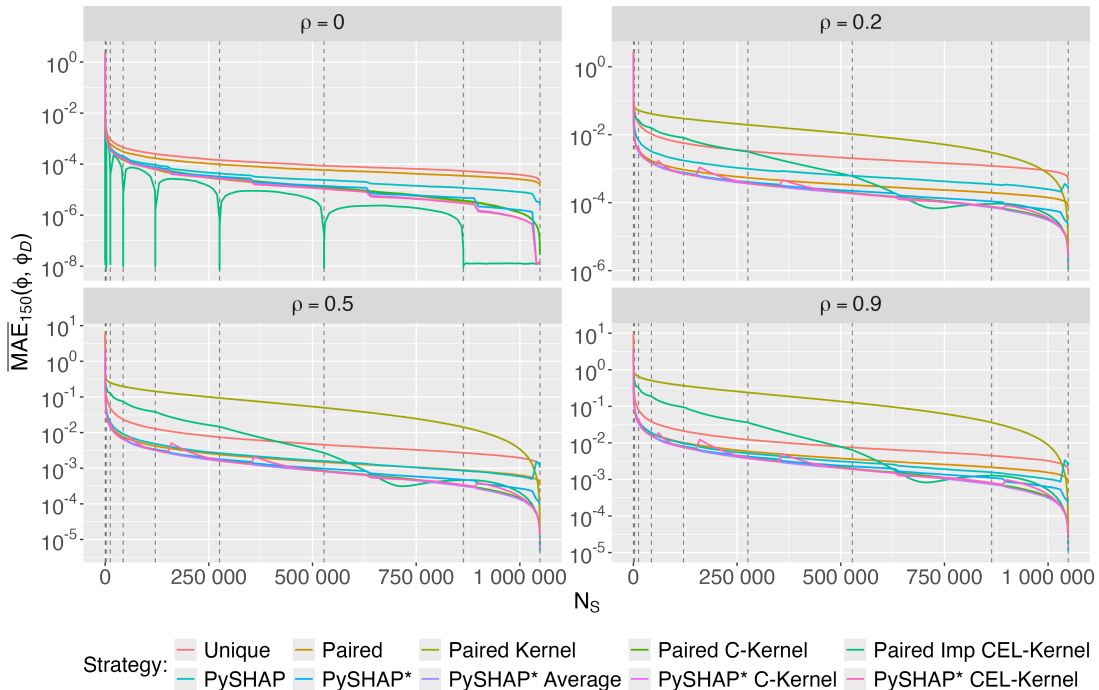


Figure 28: Linear experiment: $\text{MAE} = \overline{\text{MAE}}_{150}(\phi, \phi_{\mathcal{D}})$ for different number of coalitions $N_{\mathcal{S}}$ and dependencies levels ρ on log-scales using the strategies introduced in Appendix G. The **PySHAP* average** and **PySHAP* c-kernel** strategies are almost completely overlapping.

The first modification we propose to **PySHAP** is to always pair the coalitions, and we name this strategy **PySHAP***. Note that **PySHAP** and **PySHAP*** are equivalent when M is odd. Furthermore, we introduce the **PySHAP* average** and **PySHAP* c-kernel** strategies, which apply the averaging and correction techniques described in Sections 3.3 and 3.5, respectively. Additionally, we present the **PySHAP* cel-kernel** strategy, which uses the sampling order determined by **PySHAP*** but applies the weights introduced in Section 3.6. In Figure 26, we illustrate the sampled coalitions and normalized weights generated by the five different strategies for an increasing number of unique coalitions $N_{\mathcal{S}}$ in an $M = 10$ -dimensional setting.

The results of the **PySHAP**-based strategies for the XGBoost (Section 4.1), linear (Section 4.2), and real-world (Section 5) experiments are shown in Figures 27 to 29, respectively. We omit the 95% confidence bands in these plots because the MAE curves are now closer together than in earlier analyses presented in Sections 4 and 5, as their inclusion makes the plot more difficult to interpret. For comparison, we also include some strategies discussed in Section 3. Firstly, we observe that our **PySHAP*** strategy significantly improves upon the **PySHAP** strategy in the **SHAP** Python library when M is even. Both the **PySHAP* average** and **PySHAP* c-kernel** strategies further enhance the **PySHAP*** strategy, with their nearly identical performance –evidenced by their overlapping MAE curves. The **PySHAP* cel-kernel** strategy offers additional improvements, except for the linear experiment shown in Figure 28, where the corresponding MAE curves experience positive jumps before decreasing again with increasing $N_{\mathcal{S}}$ values. Overall, the **PySHAP* c-kernel** strategy emerges as the best-performing and most stable **PySHAP**-based strategy.

The abrupt changes in the MAE curves for the **PySHAP**-based strategies correspond to the $N_{\mathcal{S}}$ values at which two new coalition sizes are deterministically included. For example, in the $M = 10$ -dimensional setting in Figure 27, a noticeable improvement occurs at $N_{\mathcal{S}} = 268$, corresponding to the

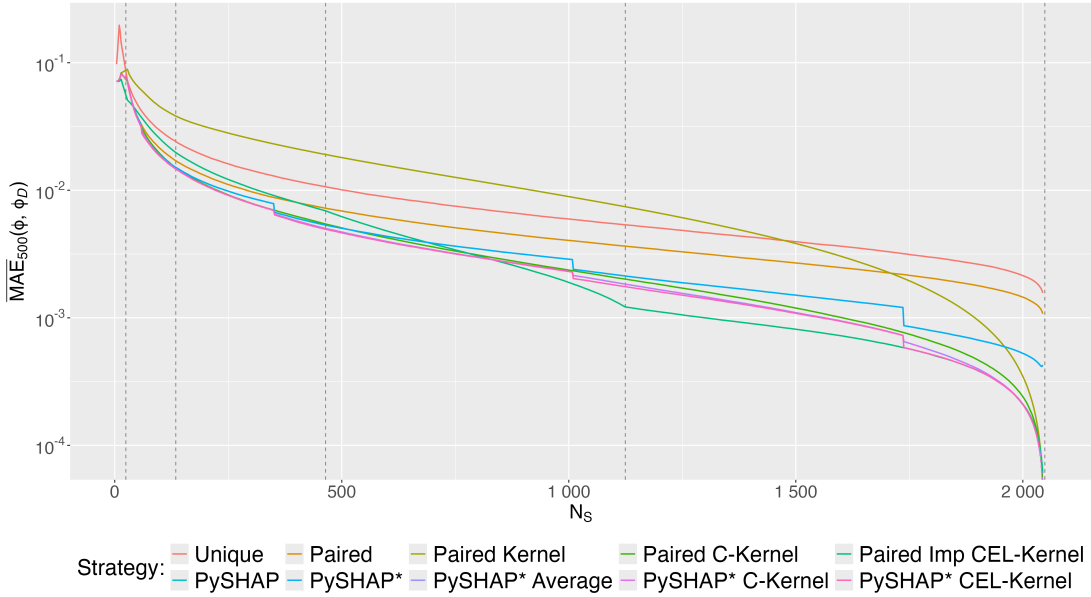


Figure 29: Red Wine experiment: $\text{MAE} = \overline{\text{MAE}}_{500}(\phi, \phi_{\mathcal{D}})$ for different number of coalitions N_S and dependencies levels ρ on log-scale using the strategies introduced in Appendix G. The **PySHAP* average** and **PySHAP* c-kernel** strategies are almost completely overlapping.

inclusion of coalitions of size two and eight, as discussed in the example above. The performance of the **PySHAP* average**, **PySHAP* c-kernel**, and **PySHAP* cel-kernel** strategies is comparable to that of the **paired c-kernel**. An advantage of the former strategies is the reduced number of repeated sampled coalitions as the number of deterministically included coalitions increases with N_S . This reduction means there are fewer possible coalitions to sample from compared to the **paired c-kernel** strategy, which considers all possible coalitions. However, it is important to note that the sampling of coalitions is computationally simple and not the primary computational burden when approximating Shapley values, as discussed in Section 6.

References

- Aas, Kjersti, Jullum, Martin, and Løland, Anders (2021a). “Explaining individual predictions when features are dependent: More accurate approximations to Shapley values”. In: *Artificial Intelligence* vol. 298, p. 103502.
- Aas, Kjersti, Nagler, Thomas, Jullum, Martin, and Løland, Anders (2021b). “Explaining predictive models using Shapley values and non-parametric vine copulas”. In: *Dependence Modeling* vol. 9, no. 1, pp. 62–81.
- Adadi, Amina and Berrada, Mohammed (2018). “Peeking Inside the Black-Box: A Survey on Explainable Artificial Intelligence (XAI)”. In: *IEEE access* vol. 6, pp. 52138–52160.
- Ancona, Marco, Oztireli, Cengiz, and Gross, Markus (2019). “Explaining deep neural networks with a polynomial time algorithm for shapley value approximation”. In: *International Conference on Machine Learning*. PMLR, pp. 272–281.
- Bifet, Albert, Read, Jesse, Xu, Chao, et al. (2022). “Linear tree shap”. In: *Advances in Neural Information Processing Systems* vol. 35, pp. 25818–25828.
- Campen, Tjeerd van, Hamers, Herbert, Husslage, Bart, and Lindelauf, Roy (2018). “A new approximation method for the Shapley value applied to the WTC 9/11 terrorist attack”. In: *Social Network Analysis and Mining* vol. 8, pp. 1–12.
- Castro, Javier, Gómez, Daniel, Molina, Elisenda, and Tejada, Juan (2017). “Improving polynomial estimation of the Shapley value by stratified random sampling with optimum allocation”. In: *Computers & Operations Research* vol. 82, pp. 180–188.
- Castro, Javier, Gómez, Daniel, and Tejada, Juan (2009). “Polynomial calculation of the Shapley value based on sampling”. In: *Computers & operations research* vol. 36, no. 5, pp. 1726–1730.
- Charnes, A, Golany, B, Keane, M, and Rousseau, J (1988). “Extremal principle solutions of games in characteristic function form: core, Chebychev and Shapley value generalizations”. In: *Econometrics of planning and efficiency*. Springer, pp. 123–133.
- Chen, Hugh, Covert, Ian C, Lundberg, Scott M, and Lee, Su-In (2023). “Algorithms to estimate Shapley value feature attributions”. In: *Nature Machine Intelligence* vol. 5, no. 6, pp. 590–601.
- (2022a). “Algorithms to estimate Shapley value feature attributions”. In: *arXiv preprint arXiv:2207.07605*.
- Chen, Hugh, Janizek, Joseph D., Lundberg, Scott, and Lee, Su-In (2020). “True to the Model or True to the Data?” In: *arXiv preprint arXiv:2006.16234*.
- Chen, Hugh, Lundberg, Scott M, and Lee, Su-In (2022b). “Explaining a series of models by propagating Shapley values”. In: *Nature communications* vol. 13, no. 1, p. 4512.
- Chen, Jianbo, Song, Le, Wainwright, Martin J, and Jordan, Michael I (2018). “L-shapley and c-shapley: Efficient model interpretation for structured data”. In: *arXiv preprint arXiv:1808.02610*.
- Chen, Tianqi, He, Tong, Benesty, Michael, Khotilovich, Vadim, Tang, Yuan, Cho, Hyunsu, et al. (2015). “Xgboost: extreme gradient boosting”. In: *R package version 0.4-2* vol. 1, no. 4, pp. 1–4.
- Cortez, Paulo, Teixeira, Juliana, Cerdeira, António, Almeida, Fernando, Matos, Telmo, and Reis, José (2009). “Using data mining for wine quality assessment”. In: *Discovery Science: 12th International Conference, DS 2009, Porto, Portugal, October 3-5, 2009 12*. Springer, pp. 66–79.
- Covert, Ian and Lee, Su-In (2021). “Improving kernelshap: Practical shapley value estimation using linear regression”. In: *International Conference on Artificial Intelligence and Statistics*. PMLR, pp. 3457–3465.

- Covert, Ian, Lundberg, Scott, and Lee, Su-In (2021). “Explaining by removing: A unified framework for model explanation”. In: *Journal of Machine Learning Research* vol. 22, no. 209, pp. 1–90.
- Covert, Ian, Lundberg, Scott M, and Lee, Su-In (2020). “Understanding Global Feature Contributions With Additive Importance Measures”. In: *Advances in Neural Information Processing Systems* vol. 33.
- Deng, Xiaotie and Papadimitriou, Christos H (1994). “On the complexity of cooperative solution concepts”. In: *Mathematics of operations research* vol. 19, no. 2, pp. 257–266.
- Duval, Alexandre and Malliaros, Fragkiskos D (2021). “Graphsvx: Shapley value explanations for graph neural networks”. In: *Machine Learning and Knowledge Discovery in Databases. Research Track: European Conference, ECML PKDD 2021, Bilbao, Spain, September 13–17, 2021, Proceedings, Part II 21*. Springer, pp. 302–318.
- Ebers, Martin (2020). “Regulating explainable AI in the European Union. An overview of the current legal framework (s)”. In: *An Overview of the Current Legal Framework (s)(August 9, 2021)*. Liane Colonna/Stanley Greenstein (eds.), *Nordic Yearbook of Law and Informatics*.
- Faigle, Ulrich and Kern, Walter (1992). “The Shapley value for cooperative games under precedence constraints”. In: *International Journal of Game Theory* vol. 21, pp. 249–266.
- Ferrante, Marco and Saltalamacchia, Monica (2014). “The coupon collector’s problem”. In: *Materials mathematics*, pp. 0001–35.
- Flajolet, Philippe, Gardy, Daniele, and Thimonier, Loÿs (1992). “Birthday paradox, coupon collectors, caching algorithms and self-organizing search”. In: *Discrete Applied Mathematics* vol. 39, no. 3, pp. 207–229.
- Frye, Christopher, Mijolla, Damien de, Begley, Tom, Cowton, Laurence, Stanley, Megan, and Feige, Ilya (2021). “Shapley explainability on the data manifold”. In: *International Conference on Learning Representations*.
- Fumagalli, Fabian, Muschalik, Maximilian, Kolpaczki, Patrick, Hüllermeier, Eyke, and Hammer, Barbara (2024). “KernelSHAP-IQ: Weighted Least-Square Optimization for Shapley Interactions”. In: *arXiv preprint arXiv:2405.10852*.
- Grabisch, Michel and Roubens, Marc (1999). “An axiomatic approach to the concept of interaction among players in cooperative games”. In: *International Journal of game theory* vol. 28, pp. 547–565.
- Herren, Andrew and Hahn, P Richard (2022). “Statistical aspects of shap: Functional anova for model interpretation”. In: *arXiv preprint arXiv:2208.09970*.
- Illés, Ferenc and Kerényi, Péter (2019). “Estimation of the Shapley value by ergodic sampling”. In: *arXiv preprint arXiv:1906.05224*.
- Jethani, Neil, Sudarshan, Mukund, Covert, Ian Connick, Lee, Su-In, and Ranganath, Rajesh (2021). “FastSHAP: Real-Time Shapley Value Estimation”. In: *International Conference on Learning Representations*.
- Jullum, Martin, Redelmeier, Annabelle, and Aas, Kjersti (2021). “Efficient and simple prediction explanations with groupShapley: A practical perspective”. In: *Italian Workshop on Explainable Artificial Intelligence 2021*. Ed. by Musto, Cataldo, Guidotti, Riccardo, Monreale, Anna, and Semeraro, Giovanni. XAI.it, pp. 28–43.
- Kroese, Dirk P, Taimre, Thomas, and Botev, Zdravko I (2013). *Handbook of monte carlo methods*. John Wiley & Sons.
- Lucas, Antoine, Scholz, Immanuel, Boehme, Rainer, Jasson, Sylvain, and Maechler, Martin (2024). *gmp: Multiple Precision Arithmetic*. R package version 0.7-4.
- Lundberg, Scott M and Lee, Su-In (2024). *shap*. Python package version 0.46.0.
- Lundberg, Scott M et al. (2020). “From local explanations to global understanding with explainable AI for trees”. In: *Nature machine intelligence* vol. 2, no. 1, pp. 56–67.

- Lundberg, Scott M. and Lee, Su-In (2017). “A unified approach to interpreting model predictions”. In: *Advances in neural information processing systems*, pp. 4765–4774.
- Maleki, Sasan (2015). “Addressing the computational issues of the Shapley value with applications in the smart grid”. PhD thesis. University of Southampton.
- Mitchell, Rory, Cooper, Joshua, Frank, Eibe, and Holmes, Geoffrey (2022). “Sampling permutations for shapley value estimation”. In: *Journal of Machine Learning Research* vol. 23, no. 43, pp. 1–46.
- Molnar, Christoph (2022). *Interpretable Machine Learning. A Guide for Making Black Box Models Explainable*. 2nd ed.
- (2023). *Interpreting Machine Learning Models With SHAP. A Guide With Python Examples And Theory On Shapley Values*. 1st ed.
- Monderer, Dov and Samet, Dov (2002). “Variations on the Shapley value”. In: *Handbook of game theory with economic applications* vol. 3, pp. 2055–2076.
- Muschalik, Maximilian, Fumagalli, Fabian, Hammer, Barbara, and Hüllermeier, Eyke (2024). “Beyond TreeSHAP: Efficient Computation of Any-Order Shapley Interactions for Tree Ensembles”. In: *Proceedings of the AAAI Conference on Artificial Intelligence*. Vol. 38. 13, pp. 14388–14396.
- Okhrati, Ramin and Lipani, Aldo (2021). “A multilinear sampling algorithm to estimate shapley values”. In: *2020 25th International Conference on Pattern Recognition (ICPR)*. IEEE, pp. 7992–7999.
- Olsen, Lars Henry Berge (2023). “Precision of individual shapley value explanations”. In: *arXiv preprint arXiv:2312.03485*.
- Olsen, Lars Henry Berge, Glad, Ingrid Kristine, Jullum, Martin, and Aas, Kjersti (2022). “Using Shapley Values and Variational Autoencoders to Explain Predictive Models with Dependent Mixed Features”. In: *Journal of Machine Learning Research* vol. 23, no. 213, pp. 1–51.
- (2024). “A comparative study of methods for estimating model-agnostic Shapley value explanations”. In: *Data Mining and Knowledge Discovery*, pp. 1–48.
- Owen, Art B. (2014). “Sobol’ indices and Shapley value”. In: *SIAM/ASA Journal on Uncertainty Quantification* vol. 2, no. 1, pp. 245–251.
- Owen, Guillermo (1972). “Multilinear Extensions of Games”. In: *Management Science* vol. 18, no. 5, P64–P79.
- Redelmeier, Annabelle, Jullum, Martin, and Aas, Kjersti (2020). “Explaining predictive models with mixed features using Shapley values and conditional inference trees”. In: *International Cross-Domain Conference for Machine Learning and Knowledge Extraction*. Springer, pp. 117–137.
- Schwalbe, Gesina and Finzel, Bettina (2023). “A comprehensive taxonomy for explainable artificial intelligence: a systematic survey of surveys on methods and concepts”. In: *Data Mining and Knowledge Discovery*, pp. 1–59.
- Sellereite, Nikolai and Jullum, Martin (2019). “shapr: An R-package for explaining machine learning models with dependence-aware Shapley values”. In: *Journal of Open Source Software* vol. 5, no. 46. Version 0.2.0, p. 2027.
- Shapley, Lloyd S. (1953). “A value for n-person games”. In: *Contributions to the Theory of Games* vol. 2, no. 28, pp. 307–317.
- Simon, Grah and Vincent, Thouvenot (2020). “A projected stochastic gradient algorithm for estimating shapley value applied in attribute importance”. In: *Machine Learning and Knowledge Extraction: 4th IFIP TC 5, TC 12, WG 8.4, WG 8.9, WG 12.9 International Cross-Domain Conference, CD-MAKE 2020, Dublin, Ireland, August 25–28, 2020, Proceedings 4*. Springer, pp. 97–115.

- Strumbelj, Erik and Kononenko, Igor (2010). “An efficient explanation of individual classifications using game theory”. In: *The Journal of Machine Learning Research* vol. 11, pp. 1–18.
- (2014). “Explaining prediction models and individual predictions with feature contributions”. In: *Knowledge and information systems* vol. 41, no. 3, pp. 647–665.
- Wang, Jiaxuan, Wiens, Jenna, and Lundberg, Scott (2021). “Shapley flow: A graph-based approach to interpreting model predictions”. In: *International Conference on Artificial Intelligence and Statistics*. PMLR, pp. 721–729.
- Wang, Rui, Wang, Xiaoqian, and Inouye, David I (2020). “Shapley Explanation Networks”. In: *International Conference on Learning Representations*.
- Williamson, Brian and Feng, Jean (2020). “Efficient nonparametric statistical inference on population feature importance using Shapley values”. In: *International Conference on Machine Learning*. PMLR, pp. 10282–10291.
- Wright, Marvin N. and Ziegler, Andreas (2017). “ranger: A Fast Implementation of Random Forests for High Dimensional Data in C++ and R”. In: *Journal of Statistical Software* vol. 77, no. 1, pp. 1–17.
- Yang, Jilei (2021). “Fast treeshap: Accelerating shap value computation for trees”. In: *arXiv preprint arXiv:2109.09847*.